# A NOVEL APPROACH TO MEASUREMENT OF THE ADHESION STRENGTH OF A SINGLE CELL ON A SUBSTRATE

# A NOVEL APPROACH TO MEASUREMENT OF THE ADHESION STRENGTH OF A SINGLE CELL ON A SUBSTRATE

By
MARIE-JOSÉE COLBERT, M.Sc

A Thesis
Submitted to the school of Graduate Studies
In Partial Fulfillment of the Requirements
For the Degree
Master of Science

McMaster University
©Copyright by Marie-Josée Colbert, 2005

MASTER OF SCIENCE (2005) McMaster University
(Physics) Hamilton, Ontario

**TITLE:** A novel approach to measurement of the adhesion strength of a single cell on a substrate

**AUTHOR:** Marie-Josée Colbert

**SUPERVISORS:** Dr Kari Dalnoki-Veress
Dr Cécile Fradin

**NUMBER OF PAGES:** xi, 53

# Table of contents

# List of figures

# List of tables

# Chapter 1: Introduction

For many years, the interactions of cells have been an important topic of research. For example, the implant industry is interested in gaining a better understanding of how cells interact with the materials used for implants in order to enhance their performance. It is also known that tumor cells interact weakly with each other, which allows a chaotic growth and a higher motility. In fact, a large fraction of biological processes go through a cell adhesion stage, such as wound healing, embryonic growth, etc. Therefore, cell adhesion studies have an interesting potential for applications.

One of the avenues to obtain information about the mechanism involved in cell adhesion is to measure its strength. In 1978 G.I. Bell presented for the first time a theoretical framework for the adhesion between cells via specific bonding[1]. A few years later E.A. Evans presented a new technique to measure the adhesion energy of a single red blood cell manipulated with a micropipette[2]. The analysis was based on the membrane deformation of the cell caused by the effect of pipette aspiration and surface adhesion. Since then, many different techniques have been employed to perform adhesion measurements, including atomic force microscopy (AFM)[3] and hydrodynamic test[4], which will be described later. Some methods are more suitable for single bond measurements, for example the AFM technique, whereas micropipette and hydrodynamic tests can be applied to whole cell studies. In the latter case, most experiments encounter the same problem, in that the adhesion energy is not directly measured. Thus, multiple interpretations of the data are based on different assumptions, which can present many sources of uncertainty.

The goal of this work was to develop a new approach to cell adhesion measurement that can avoid these problems. We chose a micropipette-based force transducer since previous studies with this tool indicated that this approach might be

highly suitable for single cell experiments[2]. Unlike some previous studies, the analysis of the results is very simple as it is based on the classical Hooke's law and Stokes' law.

This work is divided into four chapters. The first chapter describes the theory behind cell adhesion and discusses a few interpretations of the contour analysis of the cell membrane. The second chapter reviews the main techniques that have been developed and the interpretation of their results. The third chapter is focused on the description of the setup, the experimental details of the experiment and the calibration of the force transducer. The last chapter presents the typical results that are obtained from our technique. The accuracy of this method compared to others is also discussed.

# Chapter 2: Review

## 2.1 Biomembrane and lipid

### 2.1.1 Biomembrane

The biomembrane separates the cell from its surrounding environment, and thus plays a leading role in how the cell and its environment interact. It is mainly composed of different proteins and cholesterol groups inserted in a phospholipid bilayer, which is sometimes supported by a network of actin filaments forming the cytoskeleton (see figure 2.1). Attached to the bilayer are carbohydrate chains, also called polysaccharides, which are part of the extracellular matrix and are involved in many adhesion processes[5].

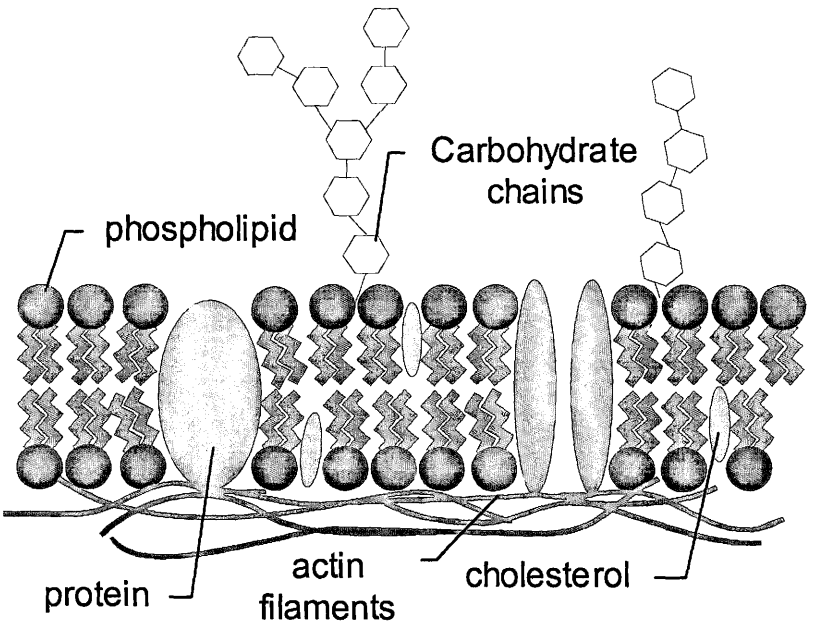


Figure 2.1: Schematic of a biomembrane

Since all these components contribute in different ways to the mechanism of cell adhesion, it is common to use the phospholipid bilayer alone as a model for the cell. This

simplified cell is called a vesicle or liposome, since it is formed from lipids (see figure 2.2).

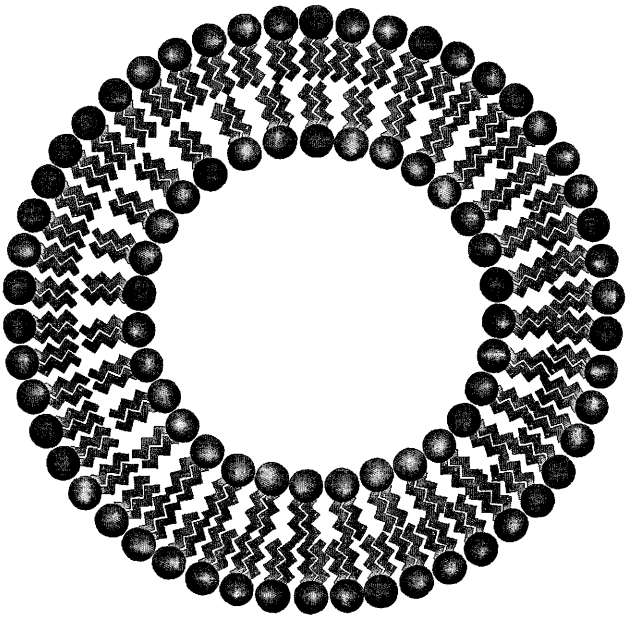

Figure 2.2: Schematic of a vesicle

### 2.1.2 Definition of lipids

Biomolecules that are soluble in fat solvents such as chloroform, acetone or benzene are known as lipids[6]. This definition includes a wide variety of molecules that are described in the table 2.1. Components of biomembranes are found in the derived lipids group: fatty acids and alcohol (sterols).

Table 2.1: Lipid groups diagram

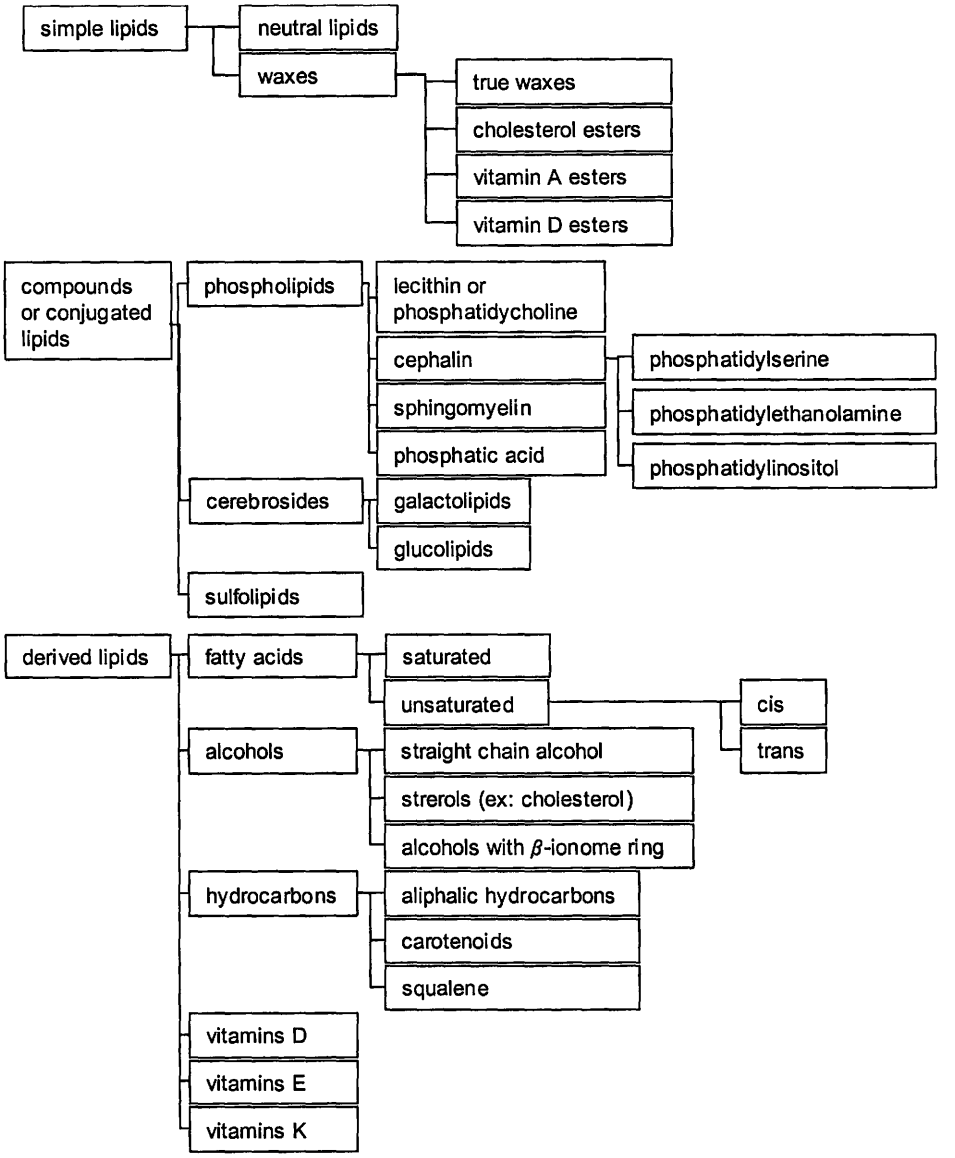


The fatty acids can be assembled and combined to a polar head group composed of a phosphoric group and a glycerol group forming the backbone of the molecule (see figure 2.3) to constitute the phospholipid group that forms the most important fraction of biomembranes. Since cells reside in an aqueous environment and are filled with water, the bilayer membrane structure is able to assemble. The assembly of lipids into bilayers or other assemblies can occur in an aqueous environment if the concentration is higher

than a critical threshold called the critical micelle concentration. Above that concentration, the repulsion between hydrophobic regions and water competes with the loss of entropy arising from the cluster formation[7]. All the neutral hydrophobic tails assemble together, so that only the polar hydrophilic heads interact with the water.

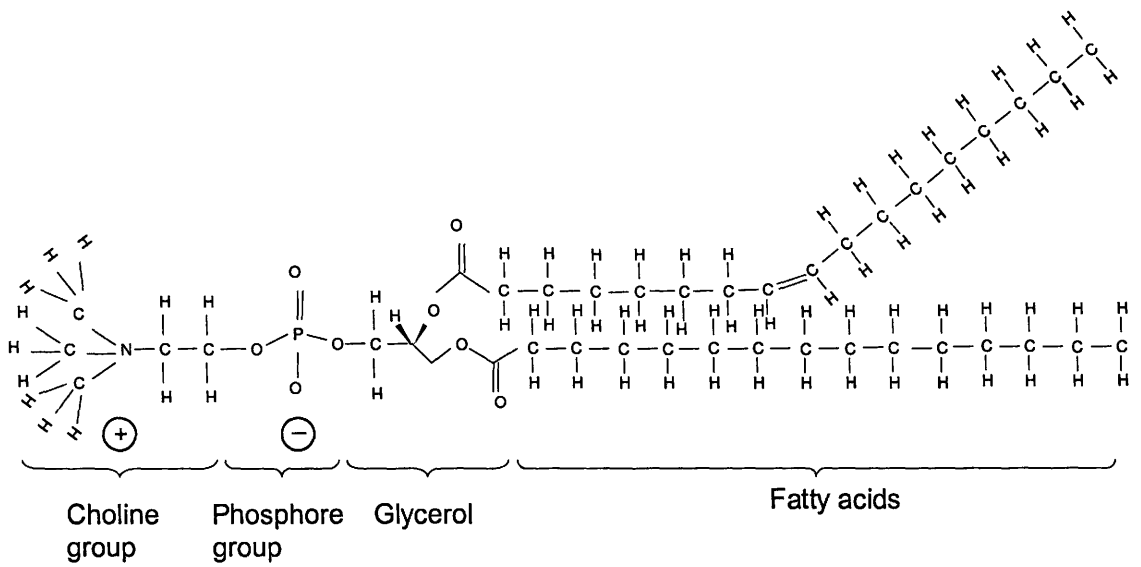


Figure 2.3: Phosphatidylcholine molecule (14:0-16:1 PC, 1-Myristoyl-2-Palmitoleoyl-Glycero-3-Phosphocholine)

The fatty acid is a hydrocarbon chain which can be either saturated with hydrogen, or unsaturated. In the unsaturated case, the chain contains a double bond in place of 2 hydrogen atoms. In nature, phospholipids are made of one saturated and one unsaturated fatty acid, both containing an even but possibly different number of carbon atoms, as shown in figure 2.3. Their names vary depending on the length of the chain and on the degree of saturation (see table 2.2 and 2.3). They can also be described with two numbers separated by a double dot (number of carbon atoms: number of double bonds).

Table 2.2: Saturated fatty acid's name[8]

| | | | |
|---|---|---|---|
| 3:0 | Propionoyl | 14:0 | Myristoyl |
| 4:0 | Butanoyl | 15:0 | Pentadecanoyl |
| 5:0 | Pentanoyl | 16:0 | Palmitoyl |
| 6:0 | Caproyl | 17:0 | Heptadecanoyl |
| 7:0 | Heptanoyl | 18:0 | Stearoyl |
| 8:0 | Capryloyl | 19:0 | Nonadecanoyl |
| 9:0 | Nonanoyl | 20:0 | Arachidoyl |
| 10:0 | Capryl | 21:0 | Heniecosanoyl |
| 11:0 | Undecanoyl | 22:0 | Behenoyl |
| 12:0 | Lauroyl | 23:0 | Trucisanoyl |
| 13:0 | Tridecanoyl | 24:0 | Lignoceroyl |

Table 2.3: Unsaturated fatty acid's name[8]

| | | | |
|---|---|---|---|
| 14:1 | Myristoleoyl | 24:1 | Nervonoyl |
| 16:1 | Palmitoleoyl | 18:2 | Linoleoyl |
| 18:1 | Oleoyl | 18:3 | Linolenoyl |
| 20:1 | Eicosenoyl | 20:4 | arachdonoyl |
| 22:1 | erucoyl | 22:6 | Docosahexenoyl |

### 2.1.3 Physical properties of lipids

The physical properties of lipids, in particular, the gel-liquid crystalline behavior are greatly influenced by the length of the chain and on the degree of saturation[9]. At lower temperatures, lipids are in a higher density state, called the gel phase, as shown in figure 2.4. As discussed by R.A.L. Jones, this state is in fact a solid state with long-ranged order, but is called gel because of its macroscopic appearance[10]. In this state, the interaction between the fatty acids is maximized and the lipids are closely packed. Butter

is an example of lipids in the gel phase at room temperature, as opposed to oil, which is in the liquid crystalline state at the same temperature[11].

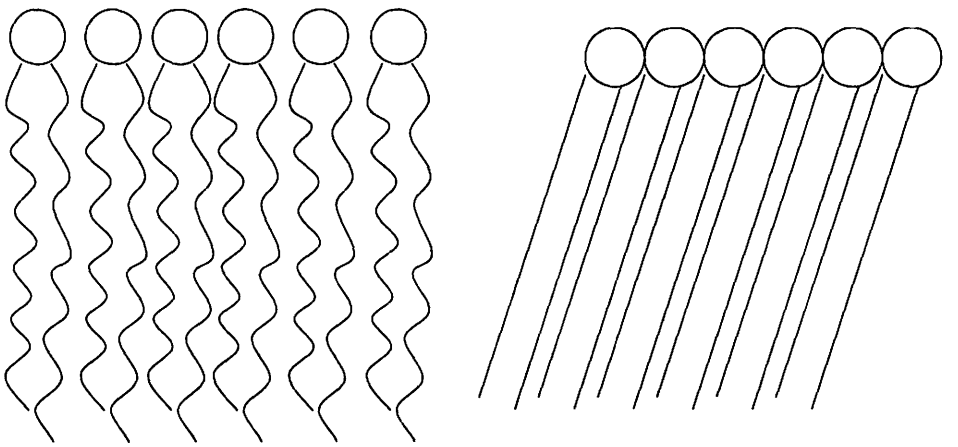

Figure 2.4: Liquid crystalline phase versus gel phase

In the case of butter, all the fatty acids are saturated, whereas the oil has one or two unsaturated chains. The double bond caused by the missing hydrogens results in a kink at the unsaturated point along the fatty acid. As a result, less energy is needed to undergo the transition into the liquid crystalline state, leading to a lower transition temperature. The interaction between the unsaturated fatty acids is not as high as that of a saturated lipid, so breaking the organization requires less energy. Thus, oil is found in a gel state at a much lower temperature than butter. Following the same reasoning, the chain length also has an influence, since a longer chain will have a higher interaction than a smaller one.

The type of saturation also plays a role in the physical properties of the lipid. The figure 2.5 illustrates the difference between the cis bond and the trans bond. The cis bond is most commonly found in nature since it is a lower energy configuration. The trans bond, as can be seen, has a smaller angle, which leads to a higher interaction with neighbors. Thus, an unsaturated trans lipid has a higher transition temperature than a

similar unsaturated cis lipid. In the same way, one understands that the degree of saturation is also important, as this will affect the angle given to the fatty acid.

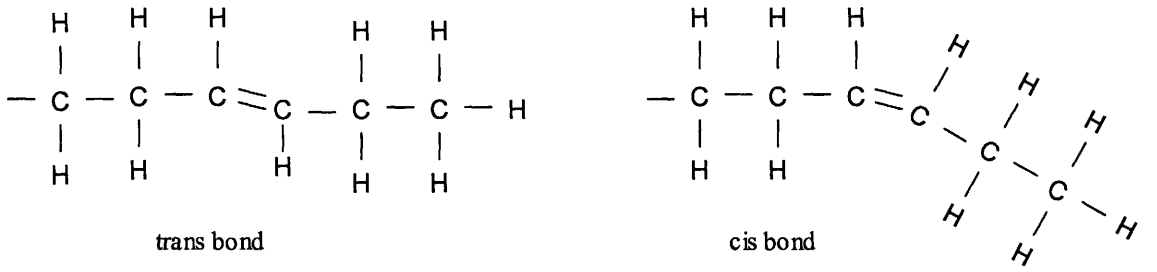


Figure 2.5: Trans bond versus cis bond

The degree of the head's polarity is another important characteristic. More polar molecules tend to have higher interaction, leading to higher liquid-gel transition temperatures as shown in table 2.4. The cholesterol content is also not to be neglected,

Table 2.4: Temperature of the gel-liquid-crystalline phase transition of phospholipids[12]

| Head group | Fatty acids* | Transition temperature (°C) |
|---|---|---|
| Phosphatidylcholine | 12:0/12:0 | -1 |
| Phosphatidylcholine | 14:0/14:0 | 23 |
| Phosphatidylcholine | 16:0/16:0 | 41 |
| Phosphatidylcholine | 18:0/18:0 | 54 |
| Phosphatidylcholine | 16:1c$\Delta^9$/16:1c$\Delta^9$ | -36 |
| Phosphatidylcholine | 18:1c$\Delta^9$/18:1c$\Delta^9$ | -20 |
| Phosphatidylethanolamine | 16:0/16:0 | 63 |
| Phosphatidylserine | 16:0/16:0 | 55 |
| Phosphatic acid | 16:0/16:0 | 67 |
| Phosphatidylglycerol | 16:0/16:0 | 41 |

*Number of carbon atoms: number of double bonds
c: cis bond, t: trans bond
$\Delta^9$: position of the double bond on the acyl chain, starting from the glycerol group

since it is thought to screen the interaction between the lipids[9]. This molecule is a neutral alcohol and it has been reported that cholesterol content higher than 30 mol% can effectively eliminate the gel phase. Examples of the transition temperature for different lipids are presented in the table 2.4. In figure 2.6 is shown a schematic of the four main head groups forming a natural biomembrane.

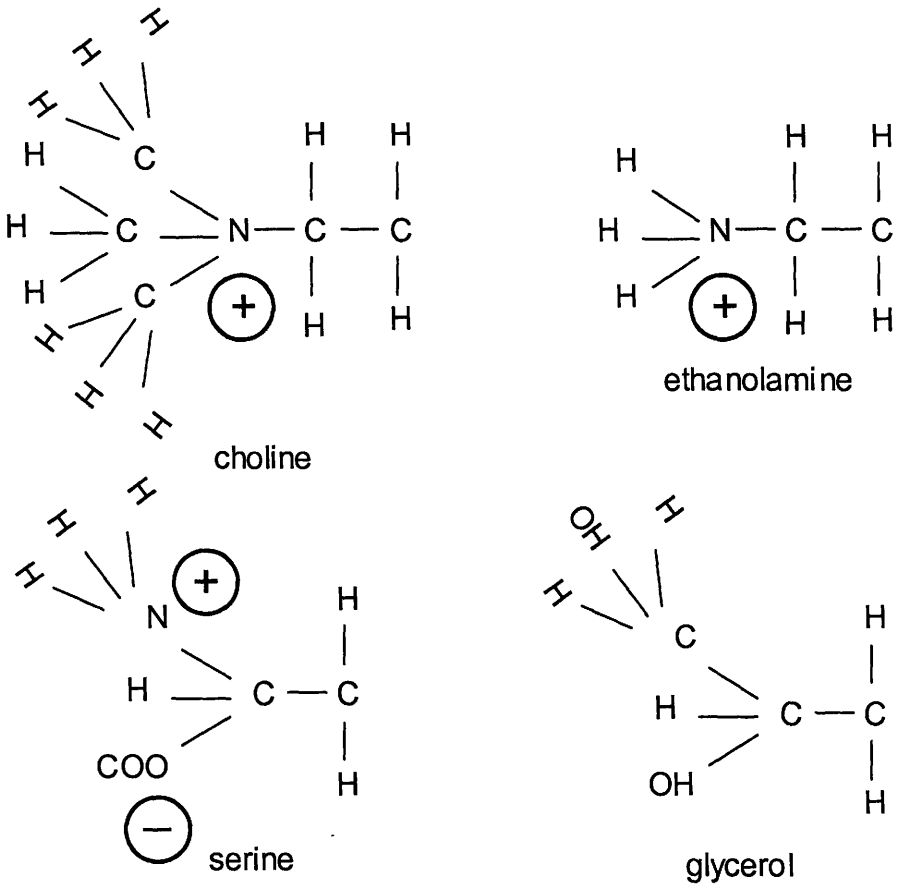


Figure 2.6: Head groups found in natural biomembrane

## 2.2 Theories of cell adhesion

### 2.2.1 Interactions involved in cell adhesion

The cell adhesion can be divided into two groups: *specific adhesion*, which is caused by the bonding between an adhesion protein embedded in the membrane and a functionalized substrate with the corresponding receptors, and *non-specific adhesion*, on which this work will be focused[13]. In the following, we summarize some details discussed in the textbook written by R.A.L. Jones[14]. It is mainly the van der Waals interaction that drives the non-specific interaction. This force appears at the atomic level, resulting from the interaction between the fluctuating dipoles of atoms. From first order perturbation theory, one finds the interaction between two uncharged atoms to be inversely proportional to the sixth power of the distance separating them. At the atomic level, the magnitude of the van der Waals interaction is not very great, but the effective force is an addition of all the interactions between pairs of atoms of the two surfaces (indicated by the subscripts) brought into contact with each other[14]:

$$U(h) = \iint \frac{-C}{r^6} \rho_1 dV_1 \rho_2 dV_2 , \tag{1}$$

where $h$ is the distance between the two surfaces, $C$ is a constant and $\rho$ is the density of the object, a membrane, in this case. For example, in the case of two membranes, the interaction is[15]:

$$U(h) = \frac{\pi \rho^2 C}{12} \left[ \frac{1}{(r+2\delta)^2} - \frac{2}{(r+\delta)^2} + \frac{1}{r^2} \right], \tag{2}$$

where $\delta$ is the thickness of the membrane. Therefore, the effects of van der Waals interactions are quite important to biological systems since they are long ranged.

In the case of electrically charged lipids, electrostatic energy can also contribute to the adhesion of a vesicle to an oppositely charged surface, or act as a repulsive force for two vesicles made of the same type of lipids. However, the electrostatic interaction is not direct when vesicles are in a solution containing dissolved ions, since it is mediated by the medium. In that case, counter-ions are attracted to the surface and create a concentration profile next to both membranes, in order to preserve the overall neutrality of the system. When the vesicles are brought in contact with each other, the concentration of ions is found to be higher between the surfaces than in the bulk solution. This causes an excess osmotic pressure which is the origin of the repulsive force.

The electrostatic interaction may be screened by ionic interactions when the vesicles are in a solution containing dissolved ions. This statement is also applicable to neutral lipids, since the membrane can adsorb ions, which will ionize it. As for the indirect electrostatic interaction, a volume of counter-ions is formed next to the membrane, resulting in an electrostatic potential $\psi$ described by the Poisson-Boltzmann equation[14]:

$$\frac{d^2\psi}{dx^2} = -\left(\frac{zen_0}{\varepsilon\varepsilon_0}\right)\exp\left(\frac{ze\psi}{k_B T}\right), \tag{3}$$

where $ze$ is the charge of the ions, $n_0$ is the ion concentration in bulk solution, $\epsilon_0$ is the vacuum permitivity, $x$ is the distance from the surface, $\epsilon$ is the permitivity of the medium, $k_B$ is the Boltzmann's constant and $T$ is the temperature. In the case of a solution containing two different ions, a general solution to this equation is:

$$\psi(x) = \psi_0 \exp(-\lambda x), \tag{3}$$

the Debye screening length is given by $1/\lambda$. At distance greater than this characteristic length, the strength of the interaction rapidly falls to zero. The Debye length is linked to the ionic strength of the solution $I$ via the expression:

$$\lambda^{-1} \propto \frac{1}{\sqrt{I}}. \tag{5}$$

Adding salt reduces the screening length, which will decrease the magnitude of the direct electrostatic interaction, which turns into a smaller osmotic pressure.

The case of vesicle-vesicle adhesion also involves depletion forces if the experiment is conducted in an aqueous solution of some polymer[16]. In that situation, the center of mass of the polymer molecules is excluded from a volume surrounding the vesicle, which is called the depletion zone. When the membranes get very close to each other, their depletion zones overlap leading to a region in the middle of the gap that has a lower concentration than the bulk. The reduced concentration leads to an osmotic effect bringing the surfaces together. The attraction energy follows[17]:

$$W_{depl} = \frac{k_B T}{a^2} \phi^{1.5}, \tag{6}$$

where $a$ is the size of the monomer, and $\phi$ is the volume fraction of polymers. In biological systems, the polymer will often be dextran or sucrose. Therefore, adding polymer in the bulk solution will increase the osmotic pressure and lead to a higher attraction between the cells.

In the case of a very strong osmotic pressure within the cell, the head group can be too spread out to shield the hydrophobic layer from the water, which would then try to eliminate the aqueous film between the membranes[18]. This hydrophobic force can add to

the depletion and van der Waals attractive forces. At lower osmotic pressure, the hydrophobic repulsion disappears and the attraction between the water and the polar heads dominates. This interaction is the called the hydration force and behaves exactly opposite to the hydrophobic force since it tends to bring more water between the interfaces[18]. Because the membrane is not rigid, it has the possibility to adopt different configurations. Thermal fluctuations of the membranes may then act as another repulsive interaction, which is called the Helfrich potential. As adhesion or some external force drives the membranes together, some configurations become inaccessible, leading to a loss of entropy. This translates to an effective potential that has the form

$$\Delta F = \frac{(k_B T)^2}{2\kappa\xi^3}\pi R^2, \tag{7}$$

where $\kappa$ is the bending rigidity constant of the membrane, $\xi$ is the amplitude of the thermal fluctuations and $R$ is the contact radius[19].

Over the years, many different theories have been developed to describe the adhesion of a vesicle or cell to a substrate. Since vesicles are usually studied in the liquid crystalline state of the lipids, the equilibrium shape is determined by minimization of the free energy[20]:

$$F = -WA_{adh} + \frac{\kappa}{2}\oint dA(C_1 + C_2)^2 + P\int dV + \Sigma\int dA. \tag{8}$$

The first term of this equation represents the positive adhesive energy, which can include all the different contributions discussed previously. $W$ is the contact potential, multiplied by the adhesion area between the surface and the vesicle. The second term is the negative bending energy, which the adhesive energy must compete with. This is multiplied by the contour integral over the adhesion patch area of the sum of the main

curvatures defining the shape of the vesicle. The two last terms are constraints imposed by the experiments, which are the conservation of the volume and of the area. $P$ and $\Sigma$ are Lagrange multipliers associated with those constraints, $P$ being related to the difference in osmotic pressure between the inside and the outside of the vesicle, and $\Sigma$ to the lateral tension.

Since membranes are in a fluid phase in a biological environment, the parallel between a liquid phospholipid membrane and a liquid drop wetting a surface is natural. It is important to note that minimizing the equation in the case of a null rigidity leads to a simple spherical cap shape. The adhesion energy is then defined by the Young-Dupré equation[20]:

$$W = \tau_m\left(1 - \cos\theta_E\right), \tag{9}$$

which describes the energy as a function of the contact angle $\theta_E$ between the droplet and the surface and interfacial tensions $\tau_m$.

### 2.2.2 Non-fixed contact angle analysis

Tordeux *et al.* base their calculation on the adhesion energy gain, the constraint on total vesicle membrane area and total enclosed volume, and the free energy cost associated with the curvature elasticity of the membrane[21]. The first step of their approach is to solve the problem of infinite adhesion. In that case, the adhesion energy is considered much greater than the bending energy. The result is a vesicle that adopts a simple spherical cap shape. This solution is similar to the model used to analyze wetting droplets, differing in the view that the contact angle is fixed by geometrical constraints instead of surface tension. A few analytical corrections can be added to the model to explain the strong finite adhesion case and to determine the equilibrium shape.

### 2.2.3 Fixed contact angle analysis

Seifert *et al.* use the same equation and the same analogy with the wetting droplet, but they set the contact angle at $\pi$ for a non-zero bending rigidity. They assume that the contact energy determines the contact curvature instead of the contact angle[22]. Therefore, any other angle would imply an infinite adhesion, since the vesicle would then adopt a spherical cap shape. Based on those assumptions, the authors present a schematic phase diagram of the contact energy as a function of the pressure, which takes into account the curvatures describing the shape of the vesicle.

### 2.2.4 Johnson-Kendall-Roberts theory

The case of specific adhesion of cells has to be treated differently when the membrane is supported by a cytoskeleton, because the system can be considered an elastic solid. Thus, the equilibrium shape is not determined by minimization of the free energy given by equation 8, but depends on the distribution of the elastic forces. In that case, Johnson-Kendall-Roberts theory gives a good description of the system[23]. The model treats the case of two spheres that are in contact with each other, one experiencing an applied load. The deformation of the bodies is caused by two different stresses: compression at the contact area, and tension at the edge. The shape observed is then not only two truncated spheres stuck together as in the case of a small contact force, but is assumed to be a profile with a contact area that meets the interface perpendicularly to the applied force (see figure 2.7).

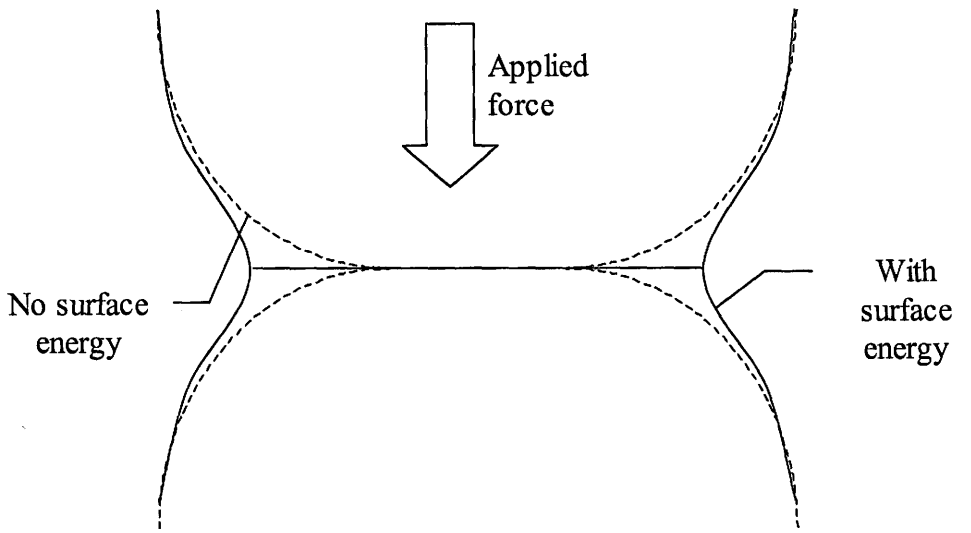


Figure 2.7: Contact between two elastic solid in presence and absence of surface energy

As the load is decreased to zero, the contact area tends toward a constant finite value because of the attractive surface forces. The total energy of the system is the sum of the stored elastic energy, the mechanical energy of the applied force and the surface energy. The equilibrium is found by minimizing the total energy with respect to the contact radius. From that condition, it is possible to calculate the radius of the contact area $a$ and the mechanical energy needed to separate the two spheres $P$ [23]:

$$a^3 = \frac{R}{K}\left(P + 3\gamma\pi R + \sqrt{6\gamma\pi RP + (3\gamma\pi R)^2}\right) \text{ and } P = \frac{3}{2}\gamma\pi R, \tag{10}$$

$$\text{with } R = \frac{R_1 R_2}{R_1 + R_2} \; ; \; K = \frac{4}{3\pi(k_1 + k_2)} \; ; \; k = \frac{1-\nu^2}{\pi E},$$

where $\gamma$ is the energy per unit of contact area, $R_n$ are the radius of the spheres, $k_n$ are the elastic constant of the spheres' materials, $\upsilon$ is the Poisson ratio and $E$ the Young's modulus of the spheres' materials.

## 2.3 Existing adhesion measurement techniques

Different methods have been developed to measure the adhesion strength between cells as well as between a cell and a specific substrate. The general procedure is often the same: a cell is stuck to a surface and then a calibrated force is applied to the adhesion force. The calibrated force is then varied until the cell detaches from the substrate, which happens when the calibrated force is equal to or greater than the adhesion force. These techniques are often combined with fluorescence spectroscopy techniques[19] and/or quartz crystal microbalance (QCM) measurements[24] to study the details of adhesion, such as the separation between the adherent surfaces, the contact angle of the cell, etc. The fluorescence and QCM techniques will not be described.

### 2.3.1 Hydrodynamic test

The peeling test is the common name used to describe the technique whereby a shear flow of a fluid is used as the calibrated force to measure the adhesion between a substrate and a cell[25]. In this experiment, the adhesive surface is one of the walls of a chamber.

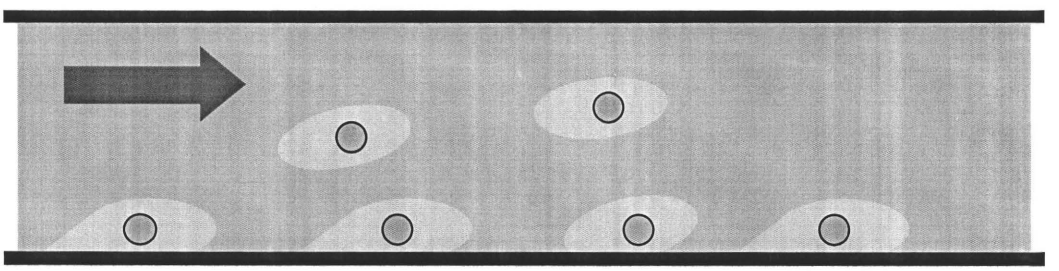

Figure 2.8: Schematic of the hydrodynamic experiment

The surface is optically transparent to allow imaging of the contact area by optical microcopy. The cells are adhering to the wall of the chamber, which is sealed except for

two holes, one that is used to inject a liquid, and the other for an exit. The force follows the Poiseuille flow[25]:

$$F = \frac{6D\eta s}{le^2}, \tag{11}$$

where $D$ is the volumetric flow rate, $\eta$ is the viscosity of the liquid, $s$ is the cell projected area, $l$ is the width of the chamber and $e$ is the space between the two surfaces forming the chamber. Optical microcopy (reflection interference contrast, fluorescence, etc) is combined with this technique to image the contact area. A model must then be constructed to analyze the deformation of the cell under the shear flow, taking into account the complex flow of the medium around the cell. This technique does not give a direct measurement of the adhesion strength, although a great advantage is the ability to obtain measurements on a statistically relevant number of cells simultaneously.

### 2.3.2 Atomic Force Microscopy

The technique using atomic force microscopy allows direct contact with the cell via its cantilever. The spring constant of the cantilever is carefully calibrated so it also serves as a force transducer. This technique is more appropriate for specific adhesion studies and was first used to measure single protein adhesion. For example, Lee *et al.* studied the interaction between steptavidin and biotin[26]. First, a glass bead coated with steptavidin is epoxied to the tip of an AFM cantilever. A mica surface is coated with biotin and immersed in a liquid chamber. The bead is then brought into contact with the coated mica surface and once contact is made, the cantilever is pulled away from the surface.

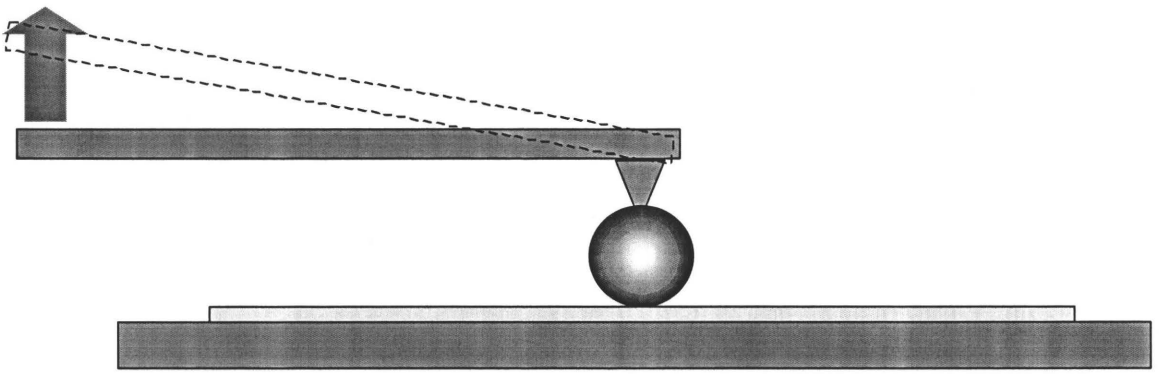

Figure 2.9: Schematic of the atomic force microscope experiment

The deflection of the cantilever is measured, which directly gives the force that is applied on the bead until it detaches from the surface. The cantilever can be extremely flexible, thus this technique can measure forces on the order of a piconewton. Some groups have tried similar experiment using murine fibroblast L929 and glass, applying a horizontal peeling force instead of a vertical force[27]. Since the cantilever directly pushes the cell, the risk of cell damage is high and the analysis encounters the same problems as those of the peeling test.

### 2.3.3 Microaspiration techniques

Evans *et al.* have developed another technique that directly interacts with cells. This technique uses a micropipette and a weak suction pressure to grab the cell. This technique is gentle enough for a vesicle and allows the study of cell-cell interaction. Once the cell has been grabbed, there are two calibrated forces that can be applied: the suction pressure, and the force due to the deformation of the vesicle itself. In the following, we discuss each method in turn.

*2.3.3.1 Microaspiration techniques utilizing suction pressure alone*

In the case of the suction pressure, the cell is put into contact with the sticky surface and the pipette is positioned so that the cell can adopt its equilibrium shape, a truncated sphere[28]. For the cell-cell adhesion test, one of the two cells is made stiff by applying a larger negative pressure and ensuring a large osmotic pressure, so that the mechanical stress will not be distributed to both cells at once, which simplifies the analysis. Then, the suction pressure applied on the soft cell is increased by a small amount, and the pipette is pulled away from the surface.

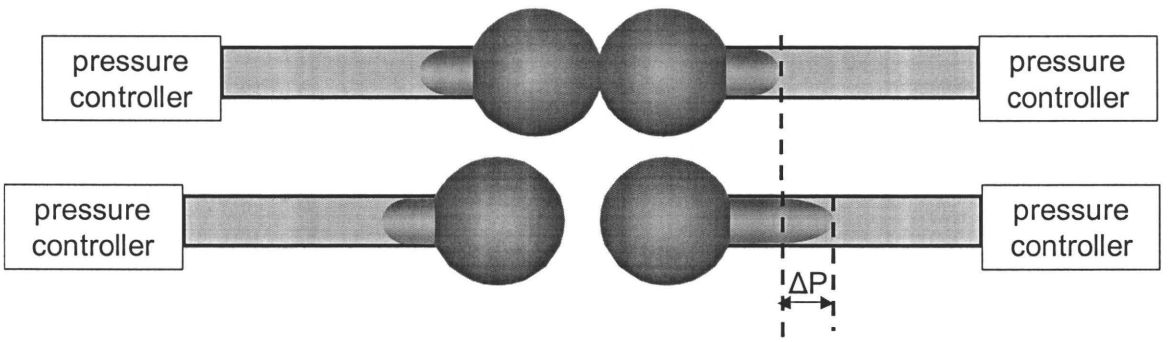


Figure 2.10: Schematic of the microaspiration experiment

If the cell remains attached to the other cell, the procedure is repeated with a slightly larger pressure. These steps are repeated until the cells detach from each other. In order to utilize the Young-Dupré equation (see equation 9), the membrane tension is needed. The pressure that causes the cell to detach is used to calculate the membrane tension via the equation[28]:

$$\tau_m \cong \frac{\Delta P R_p}{2\left(1-\frac{R_p}{R_0}\right)}, \tag{12}$$

where $\Delta P$ is the suction pressure, $R_p$ is the radius of the pipette and $R_0$ is the radius of the cell or vesicle. The contact angle is also measured, which completes the set of data necessary to use the Young-Dupré equation for the adhesion energy. This analysis approximates the bending rigidity of the cell or the vesicle at the contact perimeter to be negligible, and is not a direct measurement of the adhesion.

In the case of living cells, the procedure is the same, except that neither cells is rigid. One cell is maintained under higher negative pressure inside the pipette to ensure that the cell stays at the end of the pipette during the adhesion test, while the other experiences different pressures. JKR theory can then be used to analyze the shape of the cell and calculate the adhesion energy[17]:

$$W = \frac{2F_S}{3\pi R_m} \text{ with } R_m = \left(\frac{1}{R_1} + \frac{1}{R_2}\right)^{-1}, \tag{13}$$

where $F_S$ is the suction force and $R_m$ is the mean radius of curvature and $R_1$ and $R_2$ are radii of curvature in the two orthogonal directions of the cells, which are treated as homogeneous solid sphere.

*2.3.3.2 Microaspiration technique utilizing cell deformation*

The second way to use the micropipette technique is to analyse the deformation of the cell during the unbinding process and treat the cell as a spring.

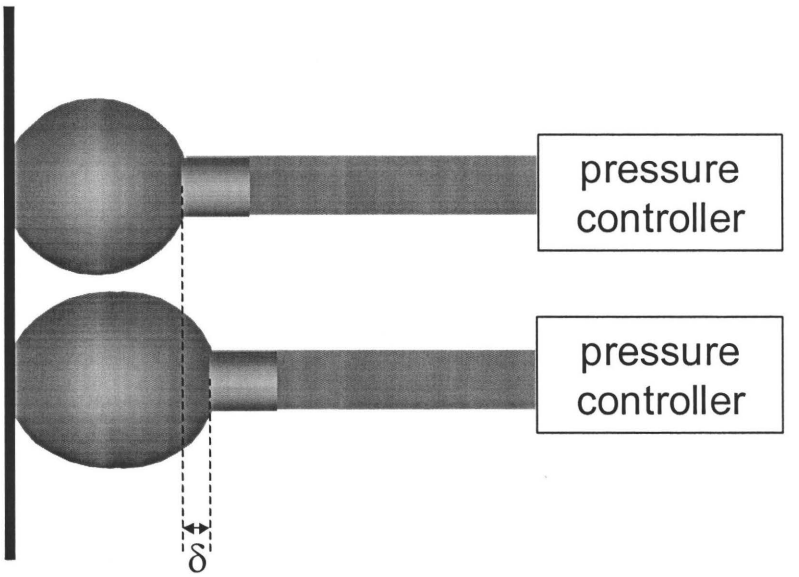


Figure 2.11: Schematic of cell used as a force transducer

For example, Pierrat *et al.* uses Johnson-Kendall-Roberts theory to describe the spring constant of a red blood cell[29]. For a small deformation, the stiffness of the cell obeys the equation:

$$k_f^{lin} = \frac{2\pi\gamma}{\ln\left(\frac{4R^2}{R_p R_c}\right)}, \tag{14}$$

where $\gamma$ is the tension applied to the membrane, $R$ is the radius of the cell, $R_c$ is the radius of the contact patch and $R_p$ is the radius of the pipette. For large deformation, they found an empirical analytical equation between the force and the stiffness:

$$\frac{f}{\pi R_p^2 \Delta P} = \frac{k_f^{lin}}{\pi R_p^2 \Delta P} - 0.1345\left|\ln(1+\delta)\right|^{3.6874}, \tag{14}$$

where $\delta$ is the elongation of the cell right before the unbinding event.

It is also possible to use a cell or a vesicle as a force transducer to measure the adhesion force between another cell and a surface. For example, Evans *et al.* use a vesicle (or a red blood cell) held by a micropipette with a polystyrene microbead chemically glued to the cell, opposite to the pipette entrance[30]. By changing the pressure inside the pipette, the spring constant of the vesicle is tuned to the needed stiffness. The bead is used as a probe to measure the elongation of the force transducer by analysis of the interference pattern produced by light diffracted from the bead. The bead can also be functionalised with a relevant receptor and be used for a specific adhesion measurement. The adhesion energy is obtained via the equations mentioned above, but the transducer can also be calibrated using optical tweezers, or magnetic tweezers if the bead is made of a paramagnetic material.

# Chapter 3: Experimental procedure

The technique developed to measure adhesion is micropipette based, and was inspired by earlier measurements by Yeung *et al.* on the effect of shear on the strength of polymer-induced flocs[31]. The pipette is pulled and bent into an L-shape so that the spring constant of the pipette can be used directly as a force transducer. Therefore, the adhesion force and energy are accessed through the measurement of the deflection of the pipette with respect to its original position, without further analysis. To do so, the base of the pipette acting as a cantilever is held fixed and the deflection is measured at the tip where the cell is held. The adhesive surface is first brought into contact with the vesicle. When the contact is achieved, the substrate is pulled away, resulting in a force on the vesicle and the pipette at the same time. The system chosen to test our approach is a phospholipid vesicle on a flat gold surface. A vesicle is a common choice because of the simplicity of its geometry and its adhesion characteristics. Preliminary experiments used a glass surface as the substrate. However, it was found that the adhesion between the vesicle and the glass was so strong that the membrane quickly ruptured when contact was made, as a result of the increase in membrane tension as the contact patch grows. Sofou *et al.* showed that that while vesicles adhere strongly to gold substrates, they don't rupture right away, as in the case of glass[32].

## 3.1 Microscope set-up

The chamber containing the vesicle was mounted over an inverted microscope (Olympus X70) placed on an anti-vibration table (Halcyonics, MOD-1). A three-dimentional micromanipulator (Narishige, model MN-151) equipped with a single axis oil hydraulic controller (Narishige, model MO-22), was mounted on the same surface supporting the microscope. The L-shaped micropipette was fixed to the micromanipulator and connected to a pressure controller: a water reservoir mounted on a

vertical micrometer translation stage. A substrate was fixed to a motorized translation stage (Newport, model MFN25cc controlled by ESP3000), which was attached atop of the microscope with the substrate inside the chamber opposite to the micropipette.

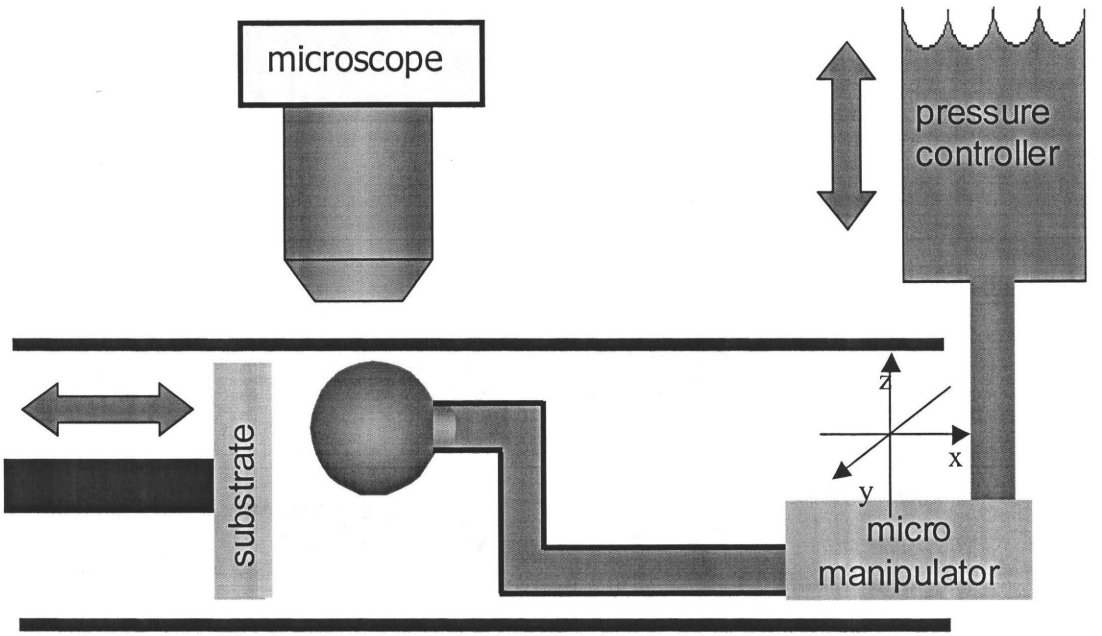


Figure 3.1: Schematic of the experimental setup

## 3.2 Sample preparation

### 3.2.1 Vesicle preparation

The first goal of this work is to measure non-specific cell adhesion, and for this, we chose lipids from the phosphocholine group (see figure 2.3) as a preliminary model, since they can form up to 20% of the membrane of a cell. This lipid is also known to be neutral and to be in the liquid crystalline state at room temperature, which simplifies the experiment. Synthetic lipids were preferred to natural lipids for the uniform length of the acyl groups, which enhances the strength of the membrane. 16:0-18:1 PC (1-Palmitoyl-

2-Oleoyl-*sn*-Glycero-3-Phosphocholine) in chloroform were purchased from Avanti Polar Lipids (Alabaster, AL) and used within a period of 6 months in order to avoid the fragility of the membrane caused by the oxidation of the lipids.

When a film of lipids is in an excess aqueous solution, the water tends to infiltrate the bilayers due to hydration and undulation forces, as well as osmotic forces. This process is called hydration and leads to the swelling of the lipid film. The film eventually breaks up and forms closed spheres to minimize the interaction of the acyl chains with the water. This process occurs over many hours and produces vesicles that are small and multilamellar.

In 1988, Dimitrov and Angelova developed a technique they called electroformation to produce giant unilamellar vesicles[33]. This procedure uses an electric field to enhance the hydration technique as discussed below. The lipid film is directly deposited on electrodes, and a DC voltage is applied. The film experiences an electro-osmotic effect immediately following the application of the voltage, causing the lipids to move for a short time. This leads to a mechanical stress on the membranes. The electrostatic interaction between the field and the lipids also accelerates the hydration process. Furthermore, it has been found that the application of an AC current can increase the efficiency of the technique. This induces a continuous periodical motion of the medium by charging and discharging the double layers. The electro-osmotic effect is reproduced at every cycle, adding to the destabilization of the membranes.

The technique we chose to produce vesicles is similar to that developed by Dimitrov and Angelova. A lipid film is spincast from a solution of lipid in chloroform (5 mg/ml) onto a glass slide (25 mm x 25 mm x 0.5 mm), precoated with a conductive layer of indium tin oxide (ITO), purchased from Delta Technologies (Stillwater, MN). The sample is then dried under vacuum for one hour. The chamber is constructed as shown in figure 3.2 so that an ITO coated glass slide forms the bottom part of the

chamber and the ITO coated glass slide covered with lipid film forms the top part. Both slides are put in direct contact with a platinum electrode and a silicone spacer. The spacers are 1.5 mm thick and are placed on opposite sides of the chamber. One sits between an electrode and the bottom glass slide, while the other sits between an electrode and the top glass slide. Two clamps hold the glass slides, the spacers and the electrodes together, forming an open chamber.

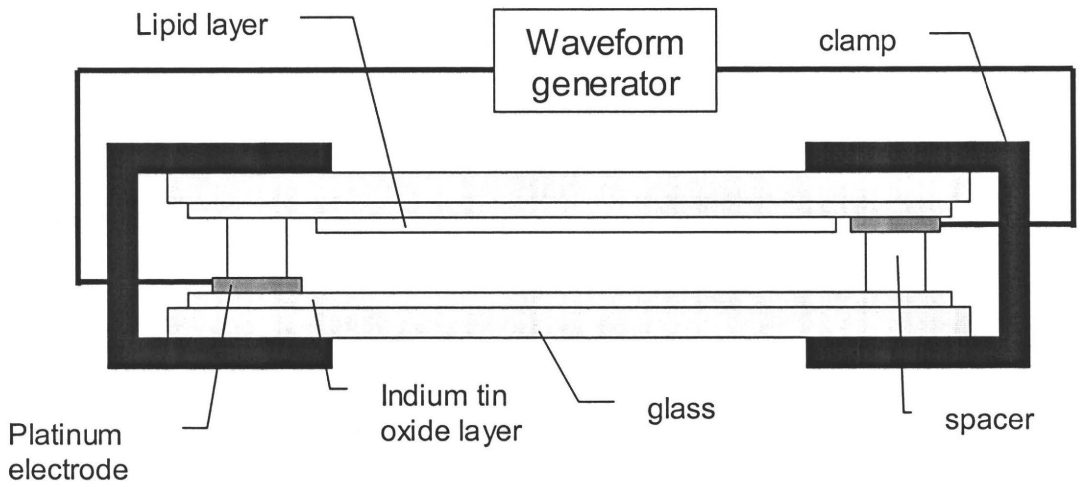


Figure 3.2: Schematic of the electroformation chamber

The chamber is filled with 0.6 ml of an aqueous sucrose solution (0.2 M) and an AC voltage (10 Hz, 2.5 Vpp) is applied for at least 2 hours via an arbitrary waveform generator (model 33120A, Agilent). After this time, vesicles with a diameter up to ~50 $\mu$m cover the top glass of the chamber (see figure 3.3). Most of the vesicles have a very thin membrane that can hardly be seen through an optical microscope. To enhance the contrast between the interior and the exterior of the vesicle, the index of refraction of the outer medium is changed by adding 0.6 ml of an aqueous solution of sodium chloride 0.2 M to the original solution. This also results in a higher density solution inside the vesicle that the surrounding medium. Thus, the bigger vesicles fall to the bottom glass slide and are directly available for the micromanipulation tests.

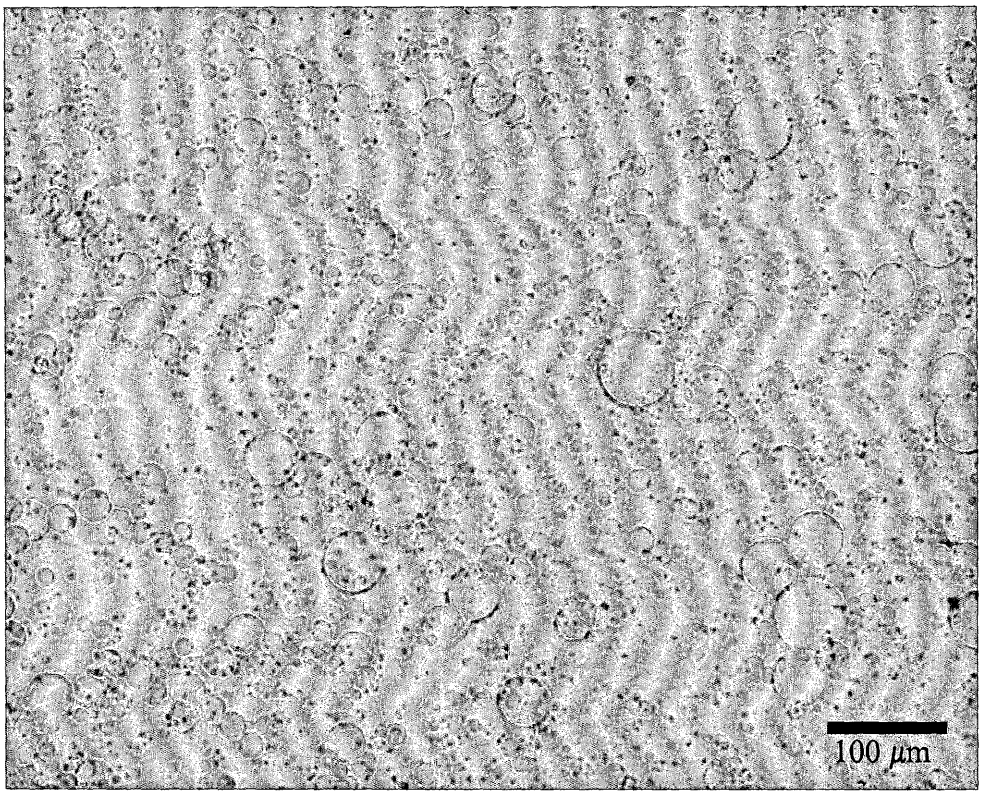


Figure 3.3: Digital microscope image of an aliquot of c16:0/18:1 PC bilayer vesicles

### 3.2.2 Micropipette shaping

The micropipettes were made out of glass capillary tubes with an inner diameter of 0.7 mm and an outer diameter of 1.0 mm (Kimble Glass Inc., model 464885). They were pulled with a commercial vertical pipette puller Kopf (David Kopf Instruments, model 720) to a diameter of 10 to 20 $\mu$m. They were then cut and shaped with a homemade microforge apparatus. The apparatus is composed of an optical microscope (Meiji techno, model SKT 28209), a three-dimensional micromanipulator (Narishige, model M-152) and a platinum wire (0,508 mm diameter, 70 mm long, ~0.4 ohm) connected to a DC power supply (Xantrex regulated DC power supply HPD 30-10). When used at higher voltages (1.3 V), the wire thermally expands and is hot enough to melt the glass pipette. Under this condition, the pipette is brought into contact with the wire using the micromanipulator until it melts and adheres to the wire. The power supply

is then abruptly turned off so that the wire quickly contracts. The contraction results in a mechanical stress to the pipette, which is cleanly cut where the contact with the wire ends in a straight line perpendicular to the pipette. At lower voltage (0.9 V) the wire cannot totally melt the glass but can still soften it enough so that the glass can be bent using a small metallic loop. For the purpose of this experiment, the micropipettes were bent as shown in figure 3.4.

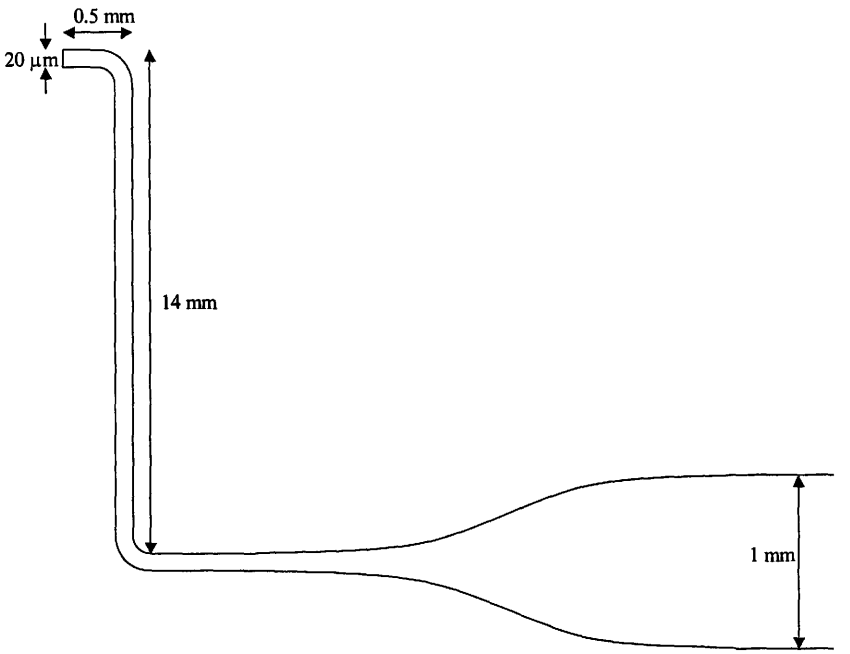


Figure 3.4: Schematic of force transducer

### 3.2.3 Substrate preparation

The substrates used consisted of gold layer (~200 nm thick) deposited onto a 0.5 mm x 1 mm x 10 mm large silicon wafer, cleaned with snow jet and left in a UV ozone chamber for one hour. The gold was sputter coated under an argon atmosphere (0.3 mbar), at a voltage of 1 kV and a current of 30 to 35 mA, for 12 minutes at a rate of 15 nm per minute (Edwards sputter coater, S150B). The substrate was then epoxied on a glass rod for mounting on a motorized translation stage. Immediately before use, the

substrate was thoroughly rinsed with methanol, followed by Milli-Q water and dried under argon or air stream.

## 3.3 Pipette deflection measurement

Figure 3.5 shows two typical images when pushing the substrate towards the pipette and as the substrate is pulled away. As can be seen, the total pipette deflection is small (~0.5 $\mu$m) and comparable to the pixel resolution. Furthermore, we need many data points within that range in order to carry out a measurement. Two different methods have been developed: one involving laser detection and the other cross-correlation image analysis.

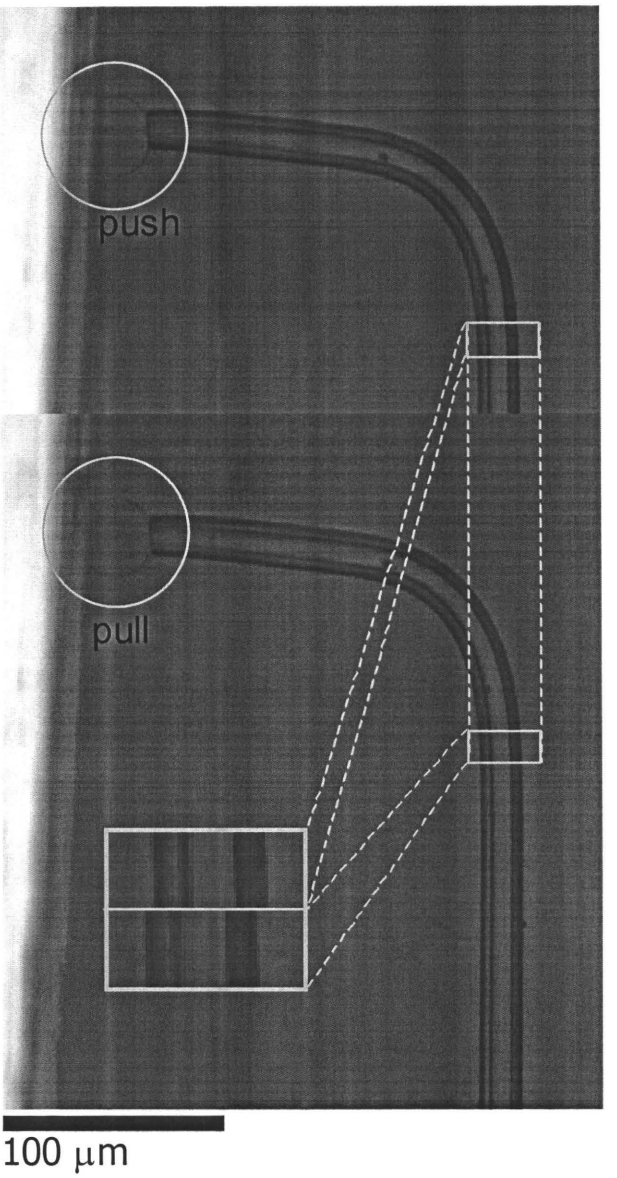


Figure 3.5: Digital microscope image of a c16:0/18:1 PC bilayer vesicle adsorbed at a gold surface and the pipette displacement just prior to the detachment event

### 3.3.1 Laser set-up

Laser detection can be used to measure the displacement, as shown in figure 3.6. It is known that when a particle is held in the focus plane of a focused laser beam, the shift in the scattering pattern is proportional to the lateral displacement of the particle[34].

A model has been developed by Gittes *et al.* that explains this phenomenon for a spherical bead. In this model the unscattered and the scattered electric field of the laser are defined when the bead is located at a position $r$ in the focal plane. When the bead moves, their value and position changes with respect to each other, as does the intensity associated with the field, which can be measured with a split photodiode.

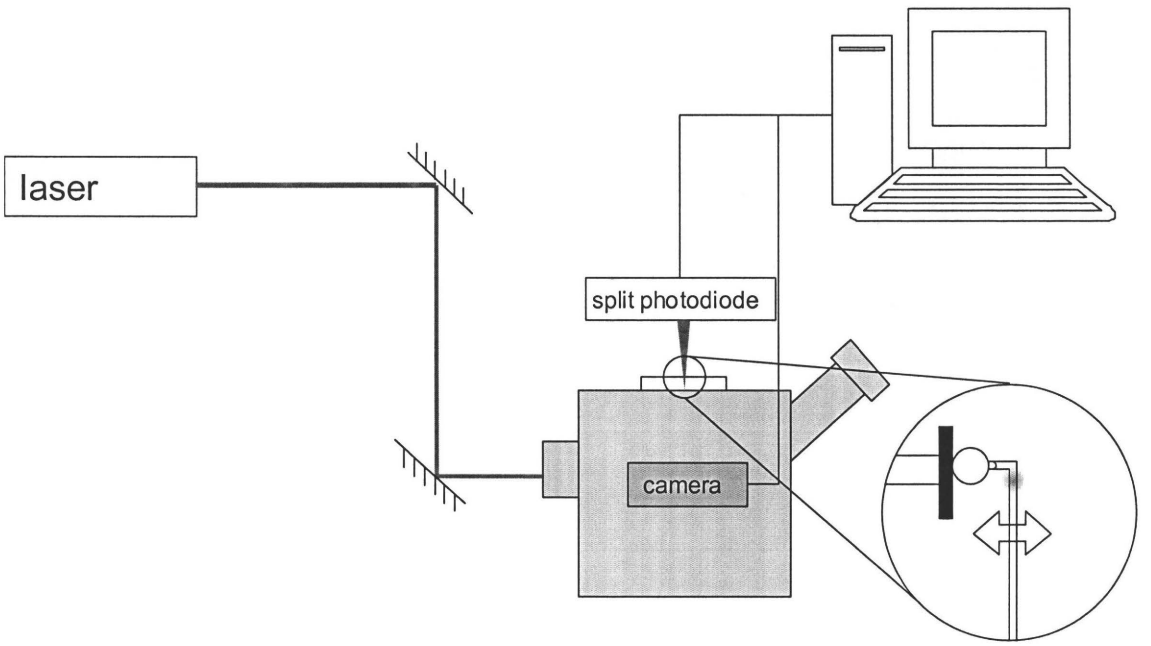


Figure 3.6: Schema of the laser detection apparatus

In our case, we use a 4 quadrant split photodiode (Newfocus, model 2901) and a laser beam (Melles Griot 25-LHP-151-249) focused onto the pipette. As the object moves in the focus plane of the beam, the value of the voltage difference of the two halves of the photodiode changes according to a curve shown in figure 3.7. This experimental calibration curve was measured using a laser beam focused on a pipette mounted on a translation stage that was then directly observed with the detector. The curve is damped at the beginning and end due to the edges of the detector and has a central portion that can be approximated as linear. The proportionality constant was found between the displacement of the pipette and the difference in intensity measured when the diffracted

laser beam was operated close to the center of the detector. For the case shown, the proportionality constant was 22.28 V/mm.

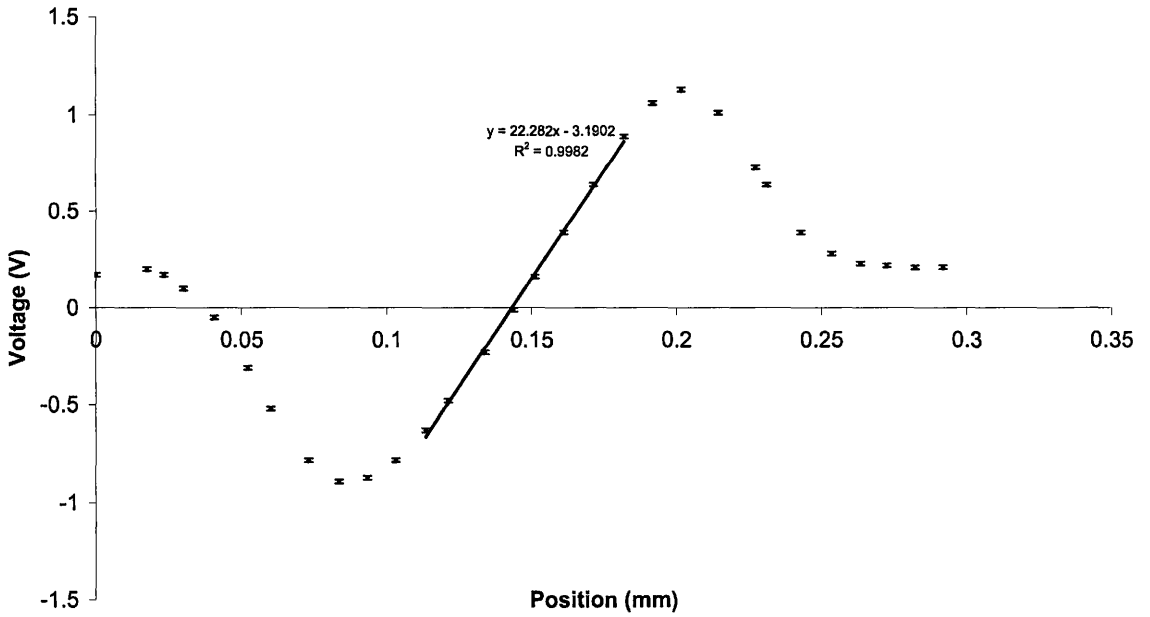


Figure 3.7: Difference in voltage measured between the two halves of the split photodiode as function of the displacement of the pipette in the focal plane of the laser

This technique measures displacement with a precision on the order of a nanometer and is thus highly suitable for this work. Unfortunately, this accuracy can be achieved only if the noise is reduced to a minimum, which has been very difficult to obtain with the actual apparatus, due to multiple reflections within the microscope.

### 3.3.2 Image analysis

The measurement of the pipette's deflection as described in this work was carried out by cross-correlation image analysis. This technique compares two images and determines the degree of correspondence between them[35]. The mathematical function is expressed as:

$$\phi_{12}(t) = \int_{-\infty}^{+\infty} f_1(x) f_2(x+t) dx \text{ or}$$

$$\phi_{12}(t) = \sum_i f_1[i] f_2[i+t] \text{ (discrete system)} \tag{16}$$

for a one-dimensional image or spectrum. First, the images are converted from color to a gray scale picture, so that every pixel becomes one step in a step function representing the intensity spectrum. The figure 3.8 is a simple example:

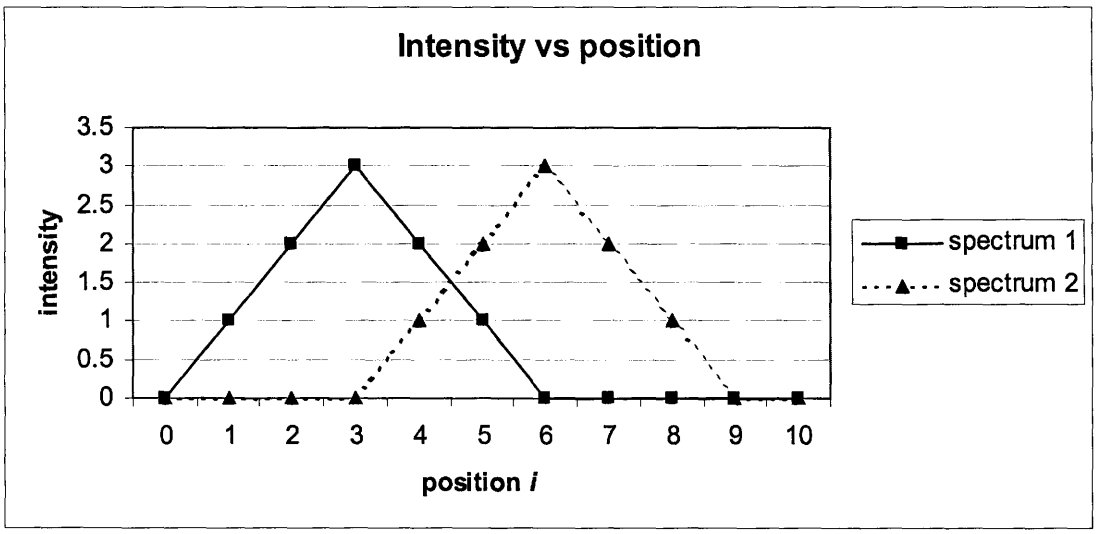


Figure 3.8: Example of an intensity spectrum and its shifted copy

The intensity value of pixel number $i$ of image 1 is multiplied by the intensity value of pixel number $i$ of image 2 ($t = 0$), forming a first spectrum of the (intensity)$^2$ as a function of the position. Afterward, image 2 is shifted by one pixel ($t = 1$) and the multiplication is repeated for all possible shifts.

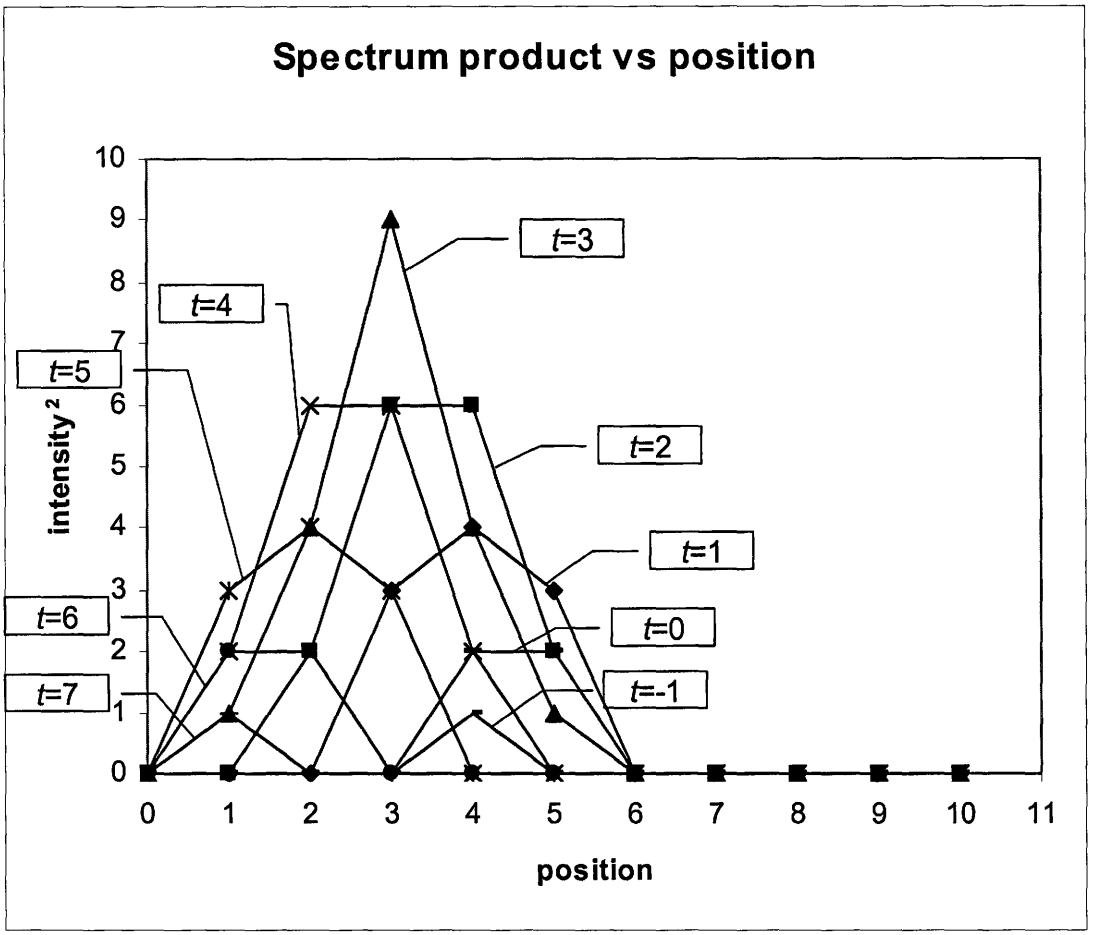


Figure 3.9: Intensity product of spectrums 1 and 2 as function of the position for different position shifts of spectrum 2

The figure 3.9 shows the result of the product for different shifts. If two peaks are very different, the product will lead to a spectrum with a low intensity (example $t = -1$ or $t = 7$). On the contrary, two similar spectrums will give a product curve with a higher intensity (example $t = 3$). The sum of the product of the intensities is taken over the position as described in equation 16 for all possible shifts so that a graph of $\Phi_{12}$ as a function of the shift $t$ is obtained. This function will have a maximum, which represents the number of pixels that image 2 needs to be shifted in order to have the highest degree of correspondence with image 1.

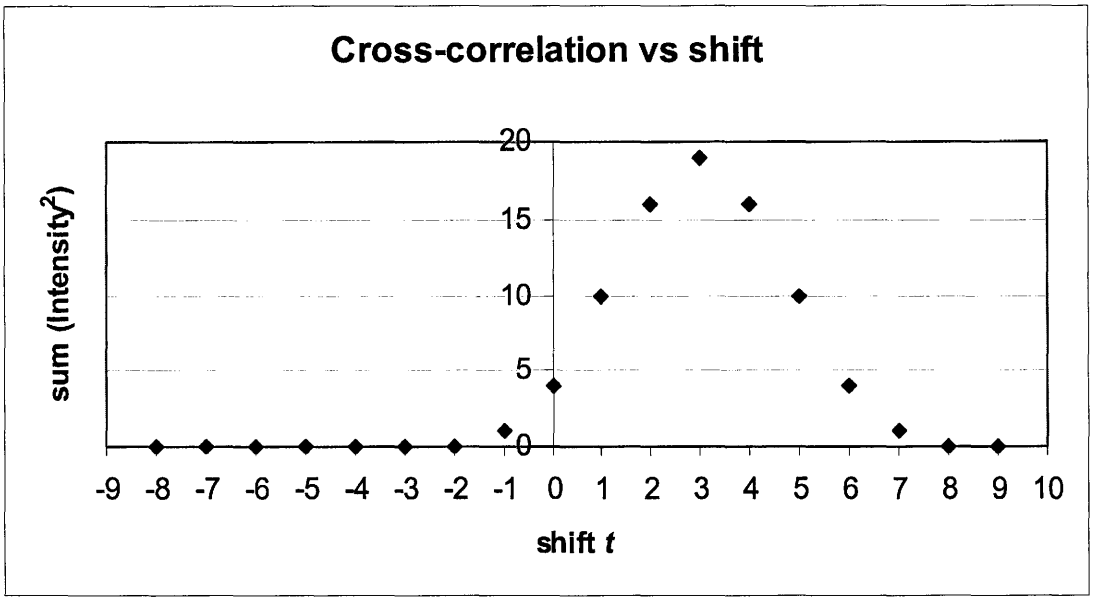


Figure 3.10: Cross-correlation function of spectrums 1 and 2 as a function of the position shift of spectrum 2

In this example, the cross-correlation function has a maximum at $t = 3$, which corresponds to the initial shift that was given to the spectrum.

It is also possible to do the same analysis with two copies of the same image. In this case, the function is called an auto-correlation. Since the two images are the same, the final function will we centered at $t = 0$. For the measure of the position of the pipette, it was most convenient to take only a segment of the image where the pipette starts to curve. For this example, $t$ represents the center of this specific region and is used as the origin when comparing to the cross-correlation result. In figure 3.11 is shown a typical example of cross-correlation functions of the pipette images for different deflections. The blue curve is the auto-correlation function, and one can see the displacements of the maxima of the cross-correlation functions.

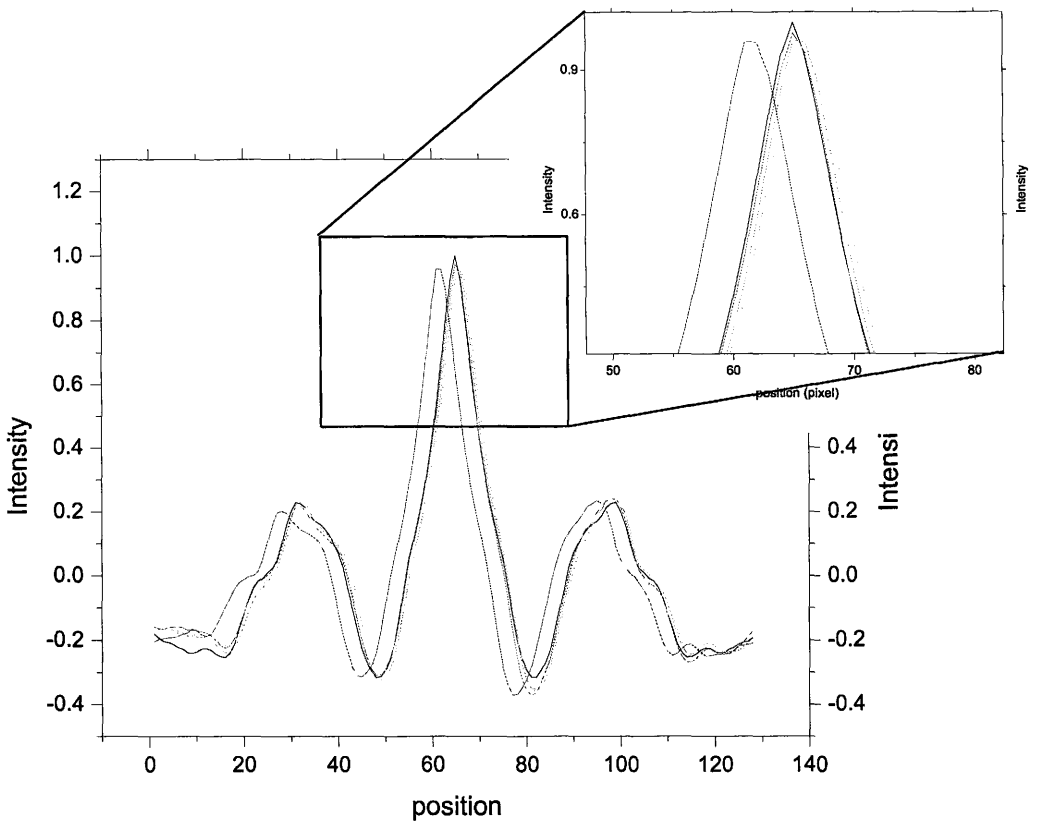


Figure 3.11: Cross-correlation function of a digital microscope image of a pipette for different pipette position

This technique allows making position measurements with a resolution better than a pixel by fitting a curve to the maximum of the correlation function and analyzing that fit based on the equation describing the fitting curve. In the example presented above, the top part of the central peak is fitted by a gaussian function. The error associated with this procedure is estimated to be 5% of a pixel. Finally, the difference in pixel number between the position of the cross-correlation function and the auto-correlation function can be converted to a distance unit using an established conversion.

## 3.4 Force transducer calibration

The pipette was calibrated through the application of a viscous force on a sphere fixed to the tip of the pipette. An open chamber was built from 2 glass cover slips, 2 silicone spacers and two clamps holding them together. The chamber was mounted on the motorized translation stage, which was attached on the top of the inverted microscope. The chamber was filled with a thick aqueous solution of sucrose (6.0 M). A few copolymer microspheres (~ 222 $\mu$m diameter, Duke Scientific Corporation, suspension 7000 series) were added, which were grabbed by the micropipette via suction through a syringe (see picture 3.12).

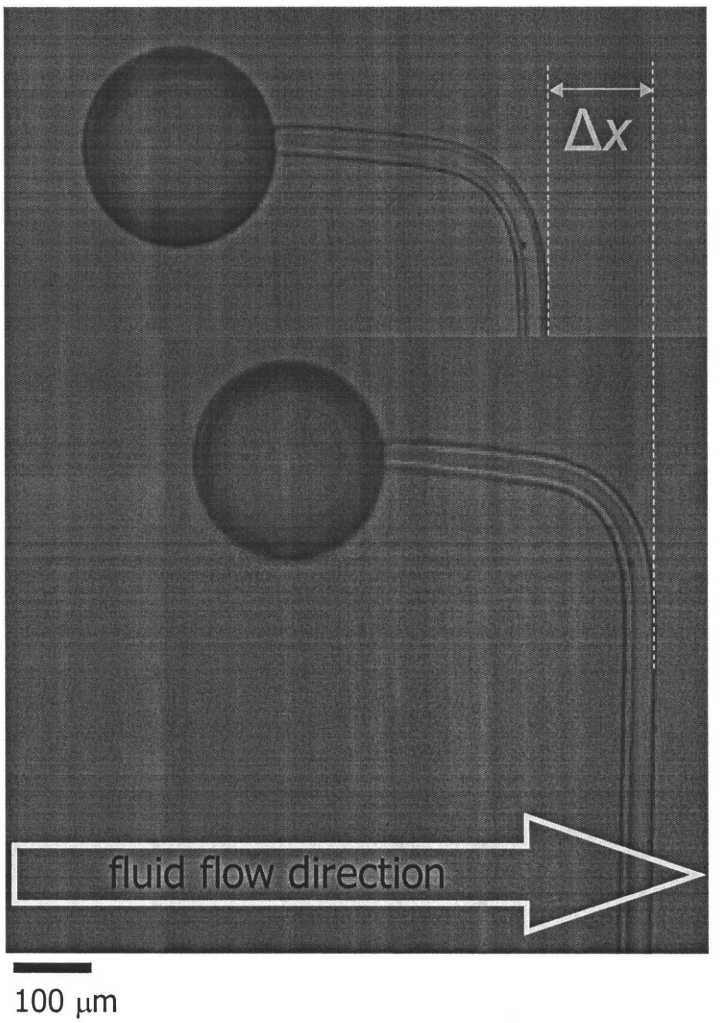


Figure 3.12: Digital microscope image of a pipette holding a polymer bead at rest and under viscous fluid flow

The chamber was then moved at a constant speed, so that equilibrium could be reached between the viscous force of the liquid on the bead and the spring force of the pipette. Using the Stokes' relation, we obtain:

$$k(\Delta x_T - \Delta x_P) = 6\pi r \eta v, \tag{17}$$

where $k$ is the spring constant of the pipette, $\Delta x_T$ is the equilibrium position of the pipette with the bead, $\Delta x_P$ is equilibrium position of the pipette without the bead, $r$ is the radius of the bead, $\eta$ is the viscosity of the liquid and $v$ is the speed of the bead with respect to the liquid[36]. A first picture was taken at rest and 10 more pictures were collected during the motion of the chamber for different velocities. The slope of the graph of the viscous force as a function of the displacement of the pipette gave the spring force (see figure 3.13).

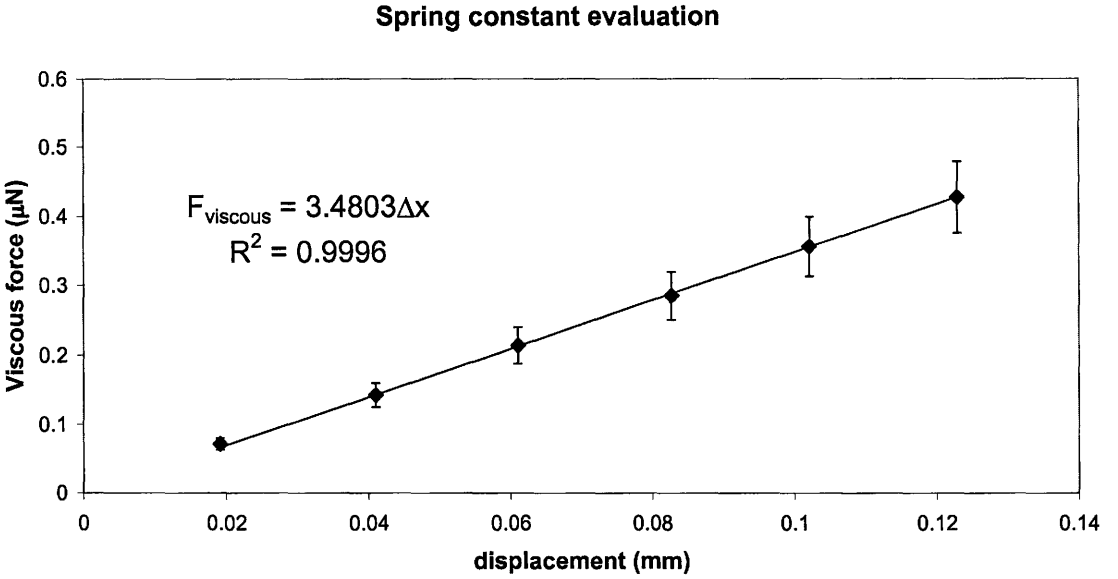


Figure 3.13: Graph of the viscous force applied on the pipette as a function of the pipette displacement

The equilibrium position $\Delta x_T$ with respect to the rest position of the pipette was measured using the cross-correlation image analysis. The same procedure was repeated, but without the bead in order to obtain $\Delta x_P$ and take into account the effect of the viscous force on the pipette and isolate the effect of the friction force on the bead. Each position measurement was averaged over 10 measurements.

The viscosity of the liquid was measured using a cylinder with 2 reasonably spaced lines filled with the thick sucrose solution at room temperature. Then, a polymer bead was dropped in the liquid, which eventually reached a terminal velocity, due to the equilibrium between the gravitational force, the viscous friction force of the liquid on the bead and the buoyancy. From this equilibrium condition, the following relation can be derived for the viscosity of the liquid:

$$\eta = \frac{2r^2(\rho_B - \rho_L)g\Delta t}{9L}, \tag{18}$$

where $r$ is the radius of the bead, $\rho$ is the density of the bead or the liquid, $t$ is the time taken for the bead to cross a distance $L$ and $g$ is the gravitational constant. The falling time was recorded and the test was repeated five times so that the average time was taken. The viscosity obtained in this way was 0.33 ± 0.04 P.

## 3.5 Labview program

A Labview program controlled the data collection of the experiment and controls the motion controller, the split photodiode and automates the image acquisition. The control panel is shown in figure 3.14. When the white arrow key at the left top of the screen is hit, the clock starts at zero. The program then goes trough a first loop of data acquisition:

- Read time;
- Read X voltage (calculate mean value over 10 points, calculate standard deviation over 10 points);
- Read Sum voltage (calculate mean value over 10 points, calculate standard deviation over 10 points);
- Read position;

Then, it produces the function "X mean voltage divided by Sum mean voltage as a function of the position", which is displayed in the last of the three windows, next to the

X voltage as a function of time window and the Sum voltage as a function of time window. When the button "Collect" is clicked, data are saved in the file specified in the "to folder" window after each reading. The saving loop goes as follow:

- Save time (second);
- Save Sum mean value (V);
- Save Sun standard deviation value (V);
- Save X mean value (V);
- Save X standard deviation value (V).
- Save position (mm);

The keys "MOVE" and "STOP MOVEMENT" give direct control of the motion of the motor. The box "Position" monitors the position of the motor with respect to an arbitrary origin, whereas the boxes "Speed" and "Relative Motion Increment" control those parameters. The speed can be set to a value between 0.0001 and 0.3 mm/sec and the direction is set by the value 1 or –1.

The settings of the camera are all accessible from the front panel. Once the key "Start/StopVideo" is hit, a preview image appears on the screen. It is possible to save a single picture with the "Capture" option to the file set in the "image path" window. The program then goes trough the following steps:

- Collect picture;
- Save picture (bitmap format);
- Save time (second);
- Save Sum mean value (V);
- Save Sum standard deviation value (V);
- Save X mean value (V);
- Save X standard deviation value (V);
- Save position (mm);

These data are saved in two different files. The file set in "Set File Path" has all data points collected when "Collect" was pressed and is useful when the pipette displacement analysis is done with the laser method. The file set in "to folder" contains only the data taken when a picture was taken, which are used for the cross-correlation image analysis.

It is also possible to take a series of pictures with "AUTO picture". The window "Capture every ? points" sets the number of loops where a picture is not saved. The loop described above is repeated and the data are saved in the two folders mentioned earlier. The first picture taken is automatically called "1" and the following picture names are incremented by 1 point.

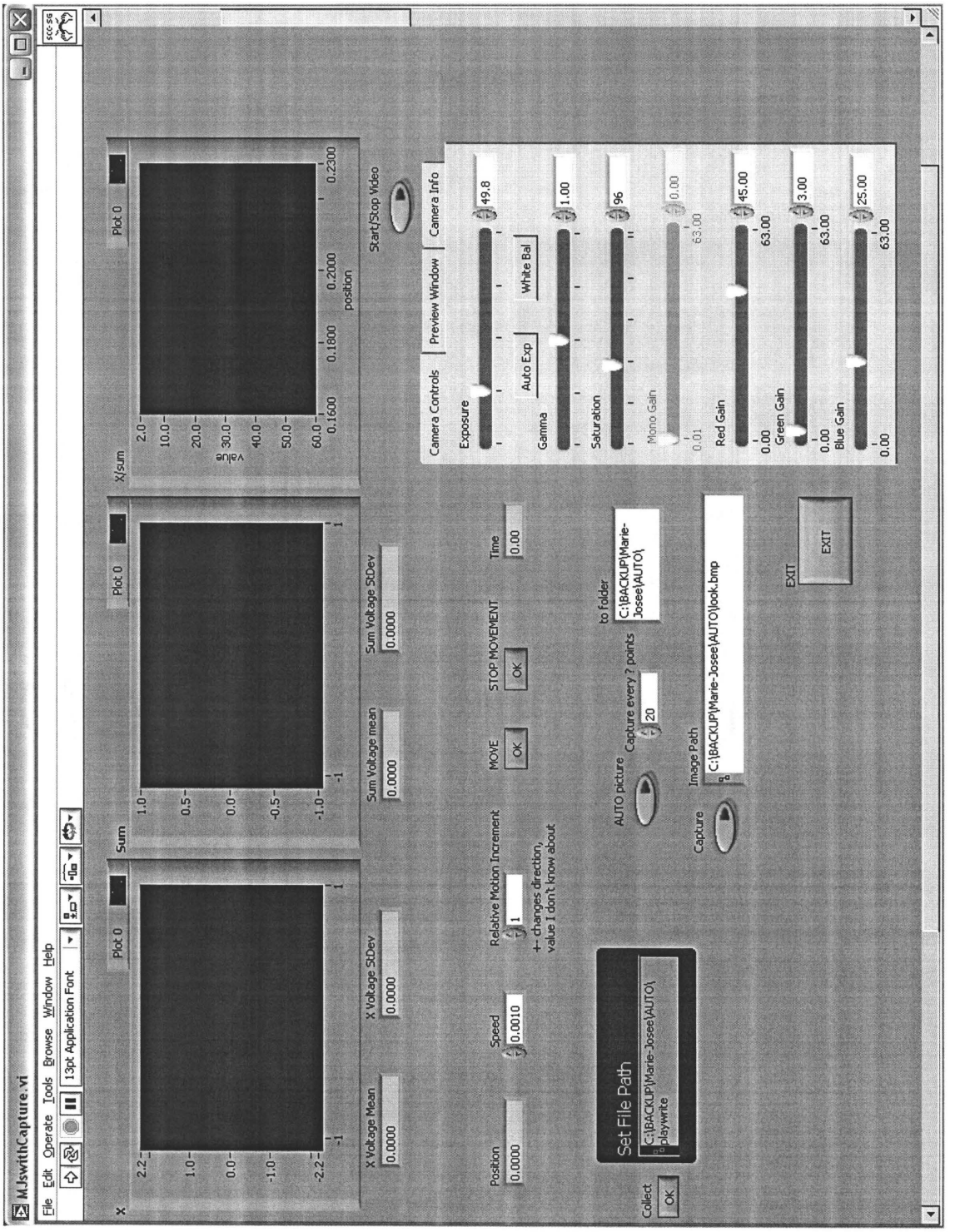


Figure 3.14: Front panel of the Labview program controlling the experiment and the data collection

# Chapter 4: Results and Discussion

## 4.1 Experimental results

The adhesion measurement was conducted as follows: the vesicle was first grabbed with the bent micropipette by applying the smallest possible negative pressure so that the vesicle barely entered the pipette. The pressure was kept constant during the whole experiment in order to keep the membrane tension as constant as possible. The cell was then brought close to the gold surface which was previously fixed to the motorized translation stage. The anti-vibration system was then turned on so that the setup was isolated from any external disturbances. The experiment could be observed in real time via the camera installed on the microscope. The substrate was brought into contact with the vesicle at a speed of 0.001 mm/s while the camera took pictures every second. When the push exerted by the surface was strong enough to visibly deform the vesicle, the motor was stopped. The vesicle was left in contact with the substrate for approximately one minute, to ensure that the water between the surface and the membrane had evacuated and that adhesion occurred[19]. The motor was then reversed and put into motion at the same speed until the cell detached from the gold substrate. As expected, the detachment event happens all at once. After the separation, the pipette went back to its original position without oscillating since the viscosity of the solution and the relatively high contact area of the pipette damp its motion. In order to ensure that the pipette was not blocked by a random particle before beginning the experiment, the pipette was calibrated using the technique described earlier at the very end of the experiment.

The pictures taken during a run were analyzed using a MatLab program. The program treats all the images within a specified file. It first displays the first image of the file. A 3 pixel wide line situated where the pipette starts curving is then selected for the auto-correlation and the cross-correlation analysis described in section 3.3.2. A gaussian

function is fit on the maximum of the correlation function, with an interval confidence of 5%. The parameters A, B and C describing the equation:

$$f(x) = A\exp\left[-\left(\frac{x-B}{C}\right)^2\right] \tag{19}$$

are written in a pre-specified file with their associated uncertainty. A typical graph obtained from this procedure is shown in figure 4.1.

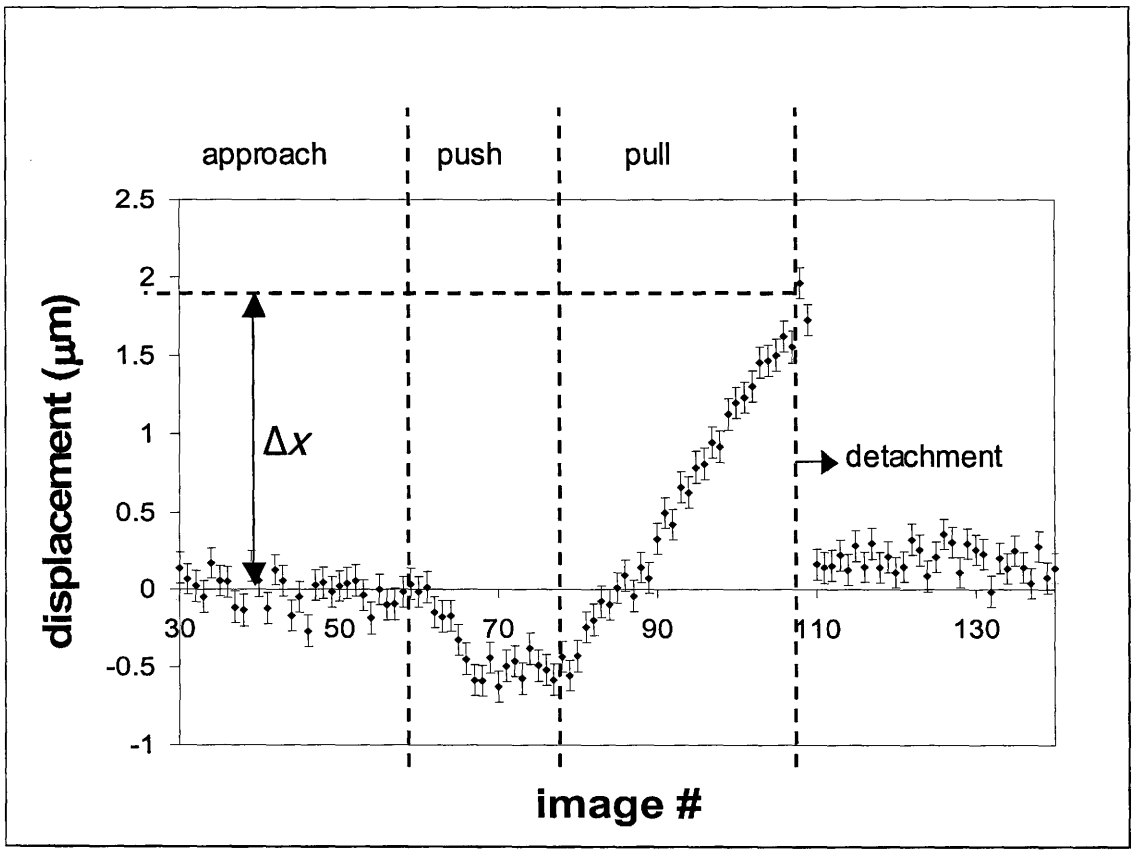


Figure 4.1: Pipette displacement induced by substrate motion as function of image number at a rate of one picture per second

This experiment was done with a pipette having a spring constant $k$ of $3.5 \pm 0.1$ nN/$\mu$m and a vesicle of a diameter of $0.039 \pm 0.002$ $\mu$m. The displacement $\Delta x$ measured was $1.8 \pm 0.2$ $\mu$m, which gives an adhesion force of $6.3 \pm 0.8$ nN. This force can be normalized to give an adhesion energy of $51 \pm 8$ nN/mm when divided by the circumference of the contact patch. The adhesion energy can also be calculated via the spring energy $\left(\frac{1}{2}k(\Delta x)^2\right)$ and gives a value of $(5.7 \pm 0.7)\text{x}10^{-15}$ J, normalized to a value of $(5 \pm 2)\text{x}10^{-11}$ J/mm$^2$, which is equal to $50 \pm 20$ nN/mm. This value and the value obtained from the spring force are the same, which may indicate that the energy dissipated in the system is negligible compare to the adhesion energy It is impossible for the moment to compare this value with published data, since previous studies have been more oriented toward vesicle-vesicle adhesion. Even though the bending energy is found to have little effects, the Young-Dupré equation cannot be applied in this case, since it doesn't take into account the external force applied to the vesicle, as seen in its non-spherical shape. However, this value is not unreasonable since Evans *et al.* have reported values of $(1\text{-}1.5)\text{x}10^{-11}$ J/mm$^2$ for the adhesion energy between two vesicles[37]. Their measurement was done with the microaspiration technique on neutral phosphocholine lipids ($L_\alpha$-PC, DMPC and SOPC).

## 4.2 Uncertainty analysis

This adhesion force measurement has a precision of 12%, which is smaller than what can be achieved with the other micropipette techniques. Indeed, Chu *et al.* report a precision of ~20% on their adhesion energy measurements when using the microaspiration technique[17]. The technique using the spring constant of the cell is even less accurate, since it gives an uncertainty of ~40%, according to Evans *et al.*[28]. However, one has to keep in mind that those results have been divided by the contact area and thus include the uncertainty from evaluating the contact area (~38%). The result

presented above is then comparable to the other techniques (40%), since the evaluation of the contact area is limited to the pixel, which translates to a micrometer precision. Other techniques should be developed in order to perform this measurement with a higher accuracy.

The main advantage this technique offers is certainly the simplicity of its analysis, its high force resolution and its versatility. Furthermore, there are very few limitations on the force range that can be measured. The stiffness of the transducer is directly related to its geometry, which can be easily adapted, depending on the desired range. The versatility of the possible applications is also interesting. It can be used to study specific or non-specific adhesion on a wide variety of substrates as well as vesicle-vesicle or cell-cell adhesion.

# Chapter 5: Conclusions

In the framework of this study, we have been able to develop a new technique for measuring the adhesion strength of a cell. This new approach allows a *direct* measurement through the spring constant of the pipette used to hold the cell. In this experiment, a sticky substrate is brought into contact with the cell. When the substrate is retracted, it pulls on the cell and on the pipette, which is displaced by a distance directly proportional to the adhesion force. The proportionality constant is the spring constant of the pipette, which is calibrated using the viscous drag of a liquid on a sphere fixed at the tip of the pipette.

The results obtained are within the nanonewton range, as expected. It was not possible to use the Young-Dupré equation to calculate the adhesion force since it requires no applied force and a known membrane tension

The main limitation on the force measurement's accuracy was the precision of the pipette's deflection measurement. We chose to use cross-correlation image analysis, which can achieve a ~10 nm precision resulting in a 12% uncertainty. This uncertainty is compares favorably to other measurement techniques. The method used to measure the radius of the contact area still needs improvement, since the uncertainty on force divided by the circumference climbs to 16%. We emphasize that this approach is in its infancy. By using the laser detection method for measuring deflection there is a potential for a two order of magnitude improvement of the force resolution. Furthermore, using fluorescence and evanescent excitation the measurement of the contact patch can easily be improved.

The versatility of the technique is also very interesting. It is suitable for cell-cell adhesion as well as for a very wide variety of substrate studies. For example, a future project will use the force transducer to study the effect of surface roughness using

ordered diblock copolymer film of different molecular weights. Finally, the range of forces that can be measured is large and can be tuned by the geometry of the pipette.

# Bibliography


[1] Bell, G.I., *Science*, **200**, 618 (1978)

[2] Evans, E.A., *Biophys J*, **30**, 265-284 (1980)

[3] Yamamotoo, A., Mishima, S., Maruyama, N., Sumita, M., *J Biomed Mater Res*, **50**, 114-124 (2000)

[4] Decave, E., Garrivier, D., Brechet, Y., Brukert, F., Fourcade, B., *Phys Rev Lett*, **89 (10)**, 108101 (2002)

[5] Boal, D. *Mechanics of the cell,* Cambridge University Press, Cambridge, 2002, p.248

[6] Deuel, H.J *The lipid:Their chemistry and biochemistry, vol1:chemistry*, Interscience publishers, inc, Nw York, 1951

[7] Cotterill, R., *Biophysics: An introduction*, John Willey and sons, ltd, England, 2002

[8] http://www.avantilipids.com/SyntheticPhosphatidylcholine.asp

[9] Vance, D.E., Vance, J.E. (editors), *Biochemistry of lipids, Lipoproteins and Membranes*, Elsevier Sciences Publishers, B.V., 1991

[10] Jones, R.A.L., *Soft condensed matter*, Oxford University Press, New-York (2002), p.148

[11] Deuel, H.J., *The lipids: Their chemistry and Biochemistry, volume 1: Chemistry*, Interscience publisher, New-York, 1951, p.50

[12] Vance, D.E, Vance, J.E., *Biochemistry of lipids, lipoproteins and membranes*, Elsevier, 1991, p.16-17

[13] Brochard-Wyart, F., deGennes, P.-G., *C.R. Physique,* **4,** (2003)

[14] Jones, R.A.L., *Soft condensed matter*, Oxford University Press, New-York (2002)

[15] Lipowsky, R., Leibler, S., *Phys Rev Lett*, **56**, 2541 (1986)

[16] Evans, E., Needham, D., *Macromolecules*, **21**, 1822-1831 (1998)

[17] Chu, Y.-S., Dufour, S., Thiery, J. P., Perez, E, Pinet, F, *Phys Rev Lett*, **94**, 028102 (2005)

[18] Bailey, S.M., Chiruvolu, S., Israelachvili, J.N., *Langmuir*, **6**, 1326 (1990)

[19] Bernard, A.-L., Guedeau-Boudeville, M.-A., Julien, L., diMeglio, J.-M., *Langmuir*, **16**, 6809-6820, (2000)

[20] Lipowsky, R., Seifert, U., *Langmuir*, **7**, 1867-1873 (1991)

[21] Tordeux, C., Fournier, J.-B., Galatola, P., *Phys Rev E*, **65**, 041912, (2002)

[22] Seifert, U., Lipowsky, R., *Phys Rev A*, **42 (8)**, 4768, (1990)

[23] Johnson, K.L., Kendall, K., Roberts, D., *ProcR Soc Lond A*, **324**, 301-313 (1971)

[24] Keller, C.A., Kasemo, B. *Biophys J*, **75**, 1397, (1998)

[25] Decave, E., Garrivier, D., Brechet, Y., Brukert, F., Fourcade, B., *Phys Rev Lett*, **89 (10)**, 108101 (2002)

[26] Lee, G.U., Kidwell, D.A., Bolton, R.J., *Langmuir*, **10**, 354-357 (1994)

[27] Yamamoto, A., Mishima, S., Maruyama, N., Sumita, M., *J Biomed Mater Res*, **50**, 114-124 (2000)

[28] Evans, E., Berk, D., Leung, A., *Biophys J*, **59**, 849-860 (1991)

[29] Pierrat, S., Brochard-Wyart, F., Nassoy, P., *Biophys J*, **87**, 2855-2869 (2004)

[30] Evans, E., Ritchie, K., Merkel, R., *Biophys J*, **65**, 2580-2587 (1995)

[31] Yeung, A., Gibbs, A., Pelton, R., *Journal of colloid and interface science*, **196**, 113-115 (1997)

[32] Sofou, S., Thomas, J.L., *Biosensors and Bioelectronics*, **18**, 445-455 (2003)

[33] Dimitrov, D.S., Angelova, M.I., *Bioelectrochemistry and Bioenergetics,* **19**, 323-336 (1988)

[34] Gittes, F., Schmidt, C.F., *Optics letters*, **23 (1)**, 7-9 (1998)

[35] Shulman, A.R., *Optical data processing*, John Wiley and Sons, Inc. 1970

[36] Jones, R.A.L. *Soft condensed matter*, Oxford University Press Inc, New-York, 2002, p.50

[37] Evans, E., Needham, D., *J. Phys. Chem.*, **91**, 4219-4228 (1987)